# Modeling of multilayer cohesive bank erosion with a coupled bank stability and mobile-bed model

Yong G. Lai[a*], Robert E. Thomas[b], Yavuz Ozeren[c],
Andrew Simon[d], Blair P. Greimann[a], and Kuowei Wu[e]

[a] Technical Service Center, U.S. Bureau of Reclamation, Denver, CO, USA
[b] Department of Geography, Environment and Earth Sciences, University of Hull, Hull, UK
[c] National Center for Computational Hydroscience and Engineering, University of Mississippi, Oxford, MS, USA
[d] Cardno-ENTRIX, Oxford, MS, USA
[e] Water Resources Planning Institute, Water Resources Agency, Wu-Fong, Taiwan, R.O.C.

* Corresponding author. Tel.: +1(303)445-2560; Fax: +1(303)445-6351; E-mail: ylai@uabr.gov.

## Abstract

Streambank erosion can be an important form of channel change in unstable alluvial environments. It should be accounted for in geomorphic studies, river restoration, dam removal, and channel maintenance projects. Recently, one-dimensional and two-dimensional flow and mobile-bed numerical models have become useful tools for predicting morphological responses to stream modifications. Most, however, either ignore bank failure mechanisms or implement only simple ad hoc methods. In this study, a coupled model is developed that incorporates a process-based bank stability model within a recently developed two-dimensional mobile-bed model to predict bank retreat. A coupling procedure that emphasizes solution robustness as well as ease-of-use is developed and described. The coupled model is then verified and validated by applying it to multilayer cohesive bank retreat at a bend of Goodwin Creek, Mississippi. Comparisons are made between the predicted and measured data, as well as results of a previous modeling study. On one hand, the study demonstrates that the use of two-dimensional mobile-bed models leads to promising improvements over that of one-dimensional models. It therefore encourages the use of multidimensional models in bank erosion predictions. On the other hand, the study also identifies future research needs in order to improve numerical modeling of complex streams. The developed model is shown to be robust and easy to apply; it may be used as a practical tool to predict bank erosion caused by fluvial and geotechnical processes.

Keywords: bank erosion; 2D mobile-bed model; coupled bank model; cohesive bank

## 1. Introduction

Streambank erosion is a natural geomorphic process occurring in all alluvial streams. Its importance as an integral part of stream geomorphology and river ecosystems has been widely recognized (Simon and Darby, 1997). It may be ecologically significant because it can create a variety of habitats for flora and fauna, contributing to ecological diversity (Environment Agency, 1999; Florsheim et al., 2008). Thus, recent restoration strategy has considered the option of removing bank protection and exposing banks to natural erosive forces (e.g., Piégay et al., 2005; van der Mark et al., 2012). In many locations disturbed by human activities, however, accelerated rates of bank retreat have caused significant land losses and elevated suspended sediment loads (Simon and Rinaldi, 2006), impacting upon water quality [1996 National Water Quality Inventory (Section 305(b) Report to Congress)]. Accelerated bank erosion can thus be a significant point source pollutant, presenting a challenge to river and reservoir managers. In some disturbed systems, streambank erosion has been found to contribute more than 50% of the total load (e.g., Wilkin and Hebel, 1982; Simon et al., 1996; Howard et al., 1998).

In response to these issues, significant effort has been expended on developing tools to predict streambank erosion and river width adjustment. Two classes of bank erosion modeling tools may be identified (Chen and Duan, 2006): empirical/analytical models and process-based models. Empirical/analytical models attempt to predict equilibrium channel width using either regime equations developed through regression on data collected from the field or extremal hypotheses that assume that alluvial channels attain equilibrium when an indicator variable reaches a maximum or minimum. Equilibrium channel width has been regressed against various parameters by, e.g., Leopold and Maddock (1953), Schumm (1968), Dunne and Leopold (1978), and Hey and Thorne (1986). Eaton (2006) recently proposed a rational regime model with explicit consideration of bank failure. Extremal hypotheses include minimum unit stream power (Yang, 1976) or stream power (Chang, 1979), maximum sediment transport efficiency (Kirkby, 1977) or capacity (White et al., 1982), minimum variance (Williams, 1978), and the principle of least action (Huang and Nanson, 2000). Although empirical/analytical models are relatively simple to use they are inappropriate for short- and medium-term predictions of unsteady geomorphic response of streams to disturbances (Simon et al., 2007).

Process-based models attempt to explicitly simulate the physical processes that are most important for bank erosion and thus aim to provide reliable short- to medium-term predictions of bank retreat in both stable and unstable channels. The ASCE (1998) provided a review of the models that existed in 1996, Rinaldi and Darby (2008) updated and expanded this review to include finite element seepage modeling, and Rinaldi and Nardi (2013) provided a review on modeling interactions between riverbank hydrology and mass failures. Langendoen and Simon (2008) provided a review focusing primarily on the geotechnical modeling elements and Motta et al. (2012) provided a review of models that linearized and nondimensionalized the two-dimensional (2D) mass and momentum equations.

Early process-based models assumed that the rate of bank retreat was proportional to the difference (or perturbation) between the depth-averaged near-bank velocity and cross-sectional mean velocity (Hasegawa, 1977; Ikeda et al., 1981). Osman and Thorne (1988) introduced probably the first process-based model to explicitly consider both lateral basal erosion and mass failure of cohesive sediments. Their method simulated both circular and planar failures for homogeneous cohesive bank retreat. The method has since been widely used with modifications and improvements. For example, Darby and Thorne (1996a) added a quasi-2D flow component to incorporate lateral shear stress, suggested a probabilistic approach to predict the streamwise length of geotechnical failures, and proposed a dimensionless parameter to assess whether a failure block would disaggregate into smaller pieces following impact with the bank face, bank toe, or water body. Later, Darby and Thorne (1996b; see also corrections published by Darby et al., 2000) added pore-water pressure and hydrostatic confining force terms and relaxed the restriction that the failure plane must pass through the toe of the bank. Mosselman (1998) incorporated an excess shear stress- and excess bank height-based bank retreat model into a quasi-steady 2D model. This model simulated equilibrium sediment transport of a single grain size, but suffered from numerical truncation when the mesh became overly skewed and/or distorted and hence required quasi-regular manual remeshing. Darby et al. (2002) incorporated the Darby and Thorne (1996a) model within that of Mosselman (1998), but found that the predictive capability of the coupled model did not significantly improve. All these models prescribed an idealized geometry and greatly simplified the bank stratigraphy, often assuming that bank material was homogeneous. Although they only simulated planar failures, the models of Simon et al. (2000), and later, Langendoen and Simon (2008), permitted the use of actual bank geometries and also accounted for multiple stratigraphic layers. Langendoen and Simon (2008) coupled a geotechnical submodel to an unsteady one-dimensional (1D) mobile-bed model called CONCEPTS (Langendoen, 2000). Their geotechnical algorithm generalizes the limit equilibrium method of Simon et al. (2000) by employing vertical slices to distribute the weight of the failure block along the failure plane and enabling the automatic detection and insertion of tension cracks. They also used a search routine to identify the minimum factor of safety. Langendoen and Simon (2008) and Langendoen et al. (2009) presented the results of a number of applications of the coupled model. Motta et al. (2012) recently coupled the geotechnical submodel within CONCEPTS to the linearized and nondimensionalized 2D mass and momentum equations and reported promising results. However, their approach is strictly valid only for the central region of mildly curved channels in which helical flow can be neglected. Motta et al. (2012) also acknowledged other simplifying assumptions such as constant discharge, constant channel width, immediate transport out of the reach of all eroded and failed bank materials, and equilibrium sediment transport with uniform bed material. They stressed the need to couple sediment transport and bank erosion submodels because of the destabilizing influence of bed degradation (or stabilizing influence of bed aggradation) and the protection potentially afforded by failed bank material.

In recent years, Darby, Rinaldi, and co-workers (Darby et al., 2007; Rinaldi and Darby, 2008; Rinaldi et al., 2008; Luppi et al., 2009) have produced a series of papers documenting the sequential and iterative use of separate models to simulate the components of the bank retreat process. For example, Rinaldi et al. (2008) used a suite of four separate models to simulate the impact of a single flood event on a bend of the Cecina River, Italy. First, they applied a commercial 2D depth-averaged flow model (Deltares Delft-3D) to predict spatiotemporal distributions of shear stress during a flood event. Second, the predicted near-bank shear stresses were inputted into a separate fluvial erosion model and the bank face and bank toe geometry were updated. Third, this updated geometry was inputted into a commercial 2D groundwater model (GeoSlope SEEP/W) to predict patterns of pore-water pressure within the streambank. Fourth, geotechnical stability was assessed with a commercial 2D rotational failure model (GeoSlope SLOPE/W) and, when cantilevers had been predicted to form, a shear-type cantilever model. Steps two to four were then repeated iteratively until the end of the flood event. Luppi et al. (2009) extended the analysis to multiple events. These studies contributed significantly to our understanding of the interactions between fluvial erosion, pore-water pressure variations, and mass failure during flood events, but their success owed much to tedious and time-consuming manual remeshing between each time step. Furthermore, interactions between the flow model, fluvial erosion, and mass failures were only loosely accounted for; no feedback occurred between the morphology of the eroding bank and the flow. Bed topographic changes were also ignored.

Despite much progress toward a fully coupled numerical model capable of simulating bank retreat, significant limitations still exist. Existing models suffer from one or several of the following: (i) use of static, rigid meshes to simulate a moving boundary problem or use of manually regenerated meshes; (ii) use of steady or quasi-steady flow models; (iii) limited consideration of the secondary currents that are characteristic of natural meander bends; (iv) simplifications to sediment transport and bed deformation submodels, making them applicable only to idealized cases (e.g., equilibrium transport of single grain sizes); (v) simplistic bank retreat models lacking key physical processes (e.g., explicitly accounting for only fluvial erosion or mass failure or neither) and requiring a number of calibration parameters to obtain realistic behaviors; and (vi) inappropriate or nonexistent coupling procedures. We believe that five elements are necessary to adequately simulate the bank retreat process: (i) a limit equilibrium geotechnical model that can evaluate the balance of forces or moments along the most critical potential failure surface that promotes and resists the downward motion of a material block; (ii) a methodology by which failed bank materials can be appropriately distributed at the bank toe or dispersed; (iii) a near-bank hydraulic model that can predict a complex 2 or 3D turbulent flow field at the spatial scale of irregular bank topography and vegetation reasonably; (iv) a robust methodology that can simulate fluvial (predominantly lateral) erosion of the bank face and bank toe; and (v) a far-field mobile-bed model that can predict sediment transport with sufficient accuracy to evaluate whether or not material eroded from the banks will be transported away from the bank. The development of a special coupling procedure so that the fully integrated model is numerically stable and user-friendly is crucial.

## 2. Description of the coupled bank stability and mobile-bed model

In this study, we develop a fully coupled flow, sediment transport, and bank stability model to predict bank retreat in alluvial streams. Our objective is to develop a general framework of a coupled model that addresses the above limitations and incorporates the five modeling elements discussed above. With the present coupled modeling framework established, some physical process submodels may be easily tested and validated in the future if further improvements are needed.

The geotechnical shear failure submodel is for multilayer streambanks with and without tension cracking. Its algorithms were documented by Langendoen (2000), Langendoen and Simon (2008), and Simon et al. (2000, 2011) and implemented in the Bank Stability and Toe Erosion Model (BSTEM) of the USDA-ARS. The BSTEM has been applied successfully in diverse alluvial environments in both static and dynamic modes (e.g., Simon et al., 2000, 2002, 2011; Simon and Thomas, 2002; Pollen and Simon, 2005; Pollen-Bankhead and Simon, 2009). In-channel fluvial processes are simulated with the extensively verified and validated 2D depth-averaged mobile-bed model SRH-2D (Lai, 2008, 2010, 2011; Lai and Greimann, 2008, 2010; Lai et al., 2011). These two models represent state-of-the-art methodologies to satisfy elements (i) and (v) listed above. A coupling procedure is developed in this study that satisfies elements (ii), (iii), and (iv) through the moving mesh Arbitrary Lagrangian-Eulerian (ALE) algorithm of Lai and Przekwas (1994).

### 2.1. Geotechnical failure algorithm

The geotechnical mass failure model adopted in this study largely follows the approach of Langendoen and Simon (2008), but with some important differences. The approach assumes that a bank consists of between one and an unlimited number of soil layers with each layer having its own geotechnical properties. Force equilibrium is invoked to compute the factor of safety. For the analysis, a potential failure block is divided into a number of vertical slices — named the vertical slice method — when the planar failure plane is known (see Fig. 1 for illustration). If J soil layers comprise the failure block, there will be J slices. To increase the accuracy of the factor of safety ($F_s$) computation, we further subdivide each layer slice into three subslices. We assume that the groundwater table within the bank is horizontal and at a constant elevation throughout the simulation. This is a relatively simple assumption that may impact modeling of the seepage effect on bank failure (Rinaldi and Nardi, 2013). We further assume that pore-water pressures are distributed hydrostatically above and below the phreatic surface, and the bank is subject to planar or cantilever shear failures. Our approach explicitly accounts for the following forces:

(1) effective cohesion, describing the electrochemical force acting between charged clay minerals;
(2) the weight of the soil block, a component of which acts to drive failure and a component of which acts to resist failure through friction;
(3) the force produced by matric suction (negative pore-water pressure) on the unsaturated part of the failure plane;

(4) the force caused by positive pore-water pressures on the saturated part of the failure plane;

(5) the hydrostatic confining force provided by the water in the channel and acting on the bank surface; and

(6) (when appropriate) interslice forces that act both normal to and parallel with the boundaries between vertical slices.

The Mohr-Coulomb shear strength criterion for unsaturated soils (Fredlund et al., 1978) quantifies forces (1) to (4) acting on the shear plane at the base of slice j as follows:

$$S_j = \frac{L_j}{F_s}\left[c'_j + (\sigma - \mu_a)_j \tan\phi'_j + (\mu_a - \mu_w)_j \tan\phi^b_j\right] \quad (1)$$

where $L_j$ = length of the slice base (m); $F_s$ = factor of safety, defined as the ratio between the resisting and driving forces acting on a potential failure block (−); c' = effective cohesion (kPa); $\sigma$ is normal stress on the shear plane at the base of the slice (kPa); $\mu_a$ = pore-air pressure (kPa); $\phi'$ is effective angle of internal friction (°); $\mu_w$ = pore-water pressure (kPa); $(\mu_a - \mu_w)$ = matric suction (kPa); and $\phi^b$ = angle describing the increase in shear strength owing to an increase in matric suction (°). For most analyses, the pore-air pressure can be set to zero. The value of $\phi^b$ varies with moisture content, but generally takes a value between 10° and 20°, with a maximum value of $\phi'$ under saturated conditions (Fredlund and Rahardjo, 1993; Simon et al., 2000).

Langendoen and Simon (2008) followed Huang (1983) for modeling force (5), the hydrostatic confining force, by assuming that the surface water within the failure block is a material with no shear strength. Hence, they extended the slip surface vertically through the water and applied a horizontal hydrostatic force on the vertical portion of the slip surface. However, application of the Langendoen and Simon (2008) algorithm is limited to cases when the failure plane angle, $\beta$, is less than $\tan^{-1}(F_s/\tan\phi')$ because at angles steeper than this, computational difficulties arise (GEO-SLOPE, 2008). At steeper failure plane angles, Langendoen and Simon (2008) merely reduced the factor of safety equation to the ratio of the shear strength of the soil to the submerged (buoyant) weight of the cantilever. However, this approach can underestimate $F_s$ if the failure block is partially submerged. Thus, in cases when the bank angle is steeper than 90°, and thence failure plane angles steeper than $\tan^{-1}(F_s/\tan\phi')$ are possible, the algorithm employed herein tests for cantilever failure by inserting $\beta$ = 90° into the Simon et al. (2000) $F_s$ equation, yielding

$$F_s = \frac{\sum_{j=1}^{J}\left(c'L + F_w \sin\alpha \tan\phi' - \mu_w L \tan\phi^b\right)_j}{\sum_{j=1}^{J}\left(W + P\cos\alpha\right)_j} \qquad (2)$$

where j = layer index; J = number of layers; $F_{w_j}$ = hydrostatic confining force acting upon the bank face within layer j per unit channel length (kNm$^{-1}$); $\alpha_j$ = mean angle of the bank face below the water surface within layer j (°); and $W_j$ = weight of layer j per unit channel length (kNm$^{-1}$). The inclusion of the $\alpha$ terms in Eq. (2) ensures that if the bank is partially or totally submerged the weights of the layers affected by water are correctly reduced irrespective of the geometry of the basal surface of the overhang.

The Langendoen and Simon (2008) algorithm is employed when $\beta < \tan^{-1}(F_s/\tan\phi')$. The calculation of $F_s$ is a four-step iterative process. First, compute the sum of the forces in the vertical direction on a slice to determine the normal force at the base of the slice, $\sigma_j L_j$:

$$\sigma_j L_j = \frac{W_j + I_{s_{j-1}} - I_{s_j} - L_j\left(c' - \mu_w \tan\phi^b\right)_j \dfrac{\sin\beta}{F_s}}{\cos\beta + \dfrac{\sin\beta \tan\phi'_j}{F_s}} \qquad (3)$$

Second, compute the sum of the forces in the horizontal direction on a slice to determine the interslice normal force, $I_{n_j}$:

$$I_{n_j} = I_{n_{j-1}} - L_j \left(c' - \mu_w \tan\phi^b\right)_j \frac{\cos\beta}{F_s} + \sigma_j L_j \left(\sin\beta - \frac{\cos\beta\tan\phi'_j}{F_s}\right) \qquad (4)$$

The calculated interslice normal forces are commonly negative near the top of the failure block. Because soil is unable to withstand large tensile stresses, herein we follow Langendoen and Simon (2008) who automatically inserted a tension crack at the last interslice boundary with tension and modified the failure block geometry accordingly. We limit the maximum tension crack depth to the depth at which Rankine's active earth pressure is equal to zero (Terzaghi and Peck, 1967). Third, model the interslice shear force and hence the direction of the resultant interslice force, using a half-sine function, $I_s = I_n \lambda \sin\left(\pi \sum_{k=1}^{j} L_k \Big/ \sum_{j=1}^{J} L_j\right)$, where k = an index and $\lambda = 0.4$ (e.g., Morgenstern and Price, 1965; GEO-SLOPE, 2008; Langendoen and Simon, 2008). Finally, sum the forces in the horizontal direction over the entire failure block, noting that the sum of the interslice normal forces over the entire block equals zero, to compute the factor of safety, $F_s$:

$$F_s = \frac{\cos\beta \sum_{j=1}^{J} L_j \left(c' + \sigma\tan\phi' - \mu_w \tan\phi^b\right)_j}{\sin\beta \sum_{j=1}^{J} \sigma_j L_j - F_w} \qquad (5)$$

The iterative procedure starts by neglecting the interslice forces and resolving the remaining forces normal to the failure plane to determine an initial estimate of $\sigma_j L_j$. This initial estimate is then used directly in Eq. (5).

The algorithm automatically computes the elevation at which the base of the failure plane emerges from the bank face and the angle of the failure plane through a global minimization procedure. Finding the global minimum is, in general, a very difficult problem (Press et al., 1992). Herein, we adopt one of the standard heuristics: at a user-defined number of failure base elevations, we isolate the failure plane angle that produces the minimum factor of safety. Once all the potential failure base locations have been searched, we select the minimum of all the local minima. This reduces our problem to a series of 1D minimization problems. We follow the recommendation of Press et al. (1992, p.395-396): 'For one-dimensional minimization (minimize a function of one variable) without calculation of the derivative, bracket the minimum…and then use Brent's method.... If your function has a discontinuous second (or lower) derivative, then the parabolic interpolations of Brent's method are of no advantage, and you might wish to use the simplest form of golden section search.' For more details of the routine and its implementation, the interested reader is referred to Press et al. (1992) §10.2. Convergence is approximately quadratic and is competitive with the method employed by Langendoen and Simon (2008).

### 2.2. In-channel mobile-bed model

We use the 2D, depth-averaged, mobile-bed model SRH-2D to simulate instream hydraulics, sediment transport, and bed deformation. Model SRH-2D has been widely used for flow and sediment transport modeling; model details may be found in Greimann et al. (2008), Lai (2010), Lai and Greimann (2010), and Lai et al. (2011). Therefore, it is only described briefly. Model SRH-2D employs an implicit, finite volume scheme to discretize the 2D, depth-averaged governing equations. We use the arbitrarily shaped element method of Lai et al. (2003) to represent bathymetry and topography. In practice, hybrid unstructured meshes, employing quadrilateral cells within main channels and triangular cells in the remaining areas, are often used because of their flexibility and increased efficiency. The discretization method is sufficiently robust that SRH-2D can simultaneously model all flow regimes (sub-, super-, and transcritical flows). Its special wetting–drying algorithm makes the model very stable to handle flows over dry surfaces. The transport of suspended, bed, or mixed load sediments for cohesive and noncohesive sediments is simulated using an unsteady, multiple-size-class, nonequilibrium sediment transport model that accounts for the effects of gravity and secondary currents on the direction of sediment transport, as well as bed armoring and sorting. Dispersive terms, resulting from the diffusion process and the depth-averaging process, are taken into consideration in the momentum equations but ignored in the sediment transport equations. Time-accurate, unsteady solution of sediment transport makes SRH-2D quite general and relatively accurate. The time discretization is the first-order Euler scheme, while the spatial discretization is the second-order scheme with damping.

## 2.3. Coupling procedure

In this study, we develop a general procedure to couple the geotechnical model to the 2D mobile-bed model. We need this procedure to accomplish three tasks. First, it needs to predict the complex flow field and sediment transport within the near-bank zone. Second, it needs to simulate fluvial erosion of the bank face and bank toe in a relatively independent fashion. Third, it needs to appropriately manage failed bank materials and simulate the basal removal process. Furthermore, while accomplishing these tasks the coupling procedure needs to be general and accurate on one hand and be simple to apply and maintain numerical stability on the other hand.

### 2.3.1. Near-bank shear stress

Two-dimensional depth-averaged models assume that vertical variations in velocity and shear stress are small relative to the horizontal (along- and across-stream) variations. Therefore, in the near bank zone, where vertical variations become significant, we need to adopt a special method to compute the shear stress distribution on the wetted bank. The ray-isovel model may be used based on a number of recent reviews (e.g., Guo and Julien, 2005; Kean and Smith, 2006a, b; Khodashenas et al., 2008; Kean et al., 2009). Kean and Smith (2006a, b) introduced a method to account for form drag at the boundaries of channels by adding a term to the streamwise momentum equation. An iterative process computes the lateral distribution of velocity and boundary shear stress in the near-bank zone by matching the near-bank distribution to that in a vertical plane at a distance one bank height from the channel margin. The need for iteration is a drawback within an already computationally intensive numerical model. Thus, we favor a noniterative geometric method to approximate the ray-isovel model (see the review by Khodashenas et al., 2008). The boundary shear stress exerted by the flow on a wetted bank node is estimated by dividing the flow area at a cross section into segments (e.g., six segments in Fig. 2). Each segment represents the flow area affected by the roughness on each wetted bank node (Einstein, 1942). Our procedure is a five-step process. First, we divide the bank and bed-affected regions by extending a bisector through the base of the bank toe to the water surface at an angle that is the average of the two nodes closest to the base of the bank toe (solid line in Fig. 2). Despite some argument about the relative merits of different approximations to the form of the divider, de Cacqueray et al. (2009) showed that the bisector method worked well for the lower part of the channel and that results away from the free surface and channel centerline were insensitive to the form of the divider. Second, we determine the mid-points between nodes on the bank face [squares between those marked (2)]. Third, we compute the absolute vertical distance between the mid-points on the bank face and bank toe and compute the total absolute vertical distance encompassed by the mid-points of the bank face and bank toe nodes. Fourth, we split the water surface between the water-bank intersect and the intersect of the line drawn in step 1 into segments with lengths that are proportional to the ratio between the absolute vertical distance between each mid-point and the total absolute vertical distance. Last, the boundary shear stress active at each node, i, is computed by $\tau_i = \tau_{toe} R_i / R_{toe}$, where $\tau_{toe}$ = bank toe shear stress (Pa), $R_i$ = hydraulic radius of the segment associated with node i (m), and $R_{toe}$ = hydraulic radius at the bank toe (m). Note that the above method is only used to obtain the shear stress distribution along the wetted bank; the toe shear stress and the water surface elevation near the bank are computed by the 2D mobile-bed model.

### 2.3.2. Fluvial erosion

On each bank section, the toe node is the only mesh point that simultaneously experiences both vertical and lateral erosion. The mobile-bed model computes the vertical change of the toe node (if any), but we need an approach to compute the lateral erosion of all wetted bank nodes. For noncohesive sediments, the control volume method proposed by Hasegawa (1981), and subsequently adopted by Nagata et al. (2000), Duan et al. (2001), and Chen and Duan (2006), is perhaps theoretically appealing. However, large uncertainties may result if a bank face is steep because in 2D models the number of mesh nodes used to define the bank is usually few. In this study, we instead compute the lateral retreat of wetted bank faces with the excess shear stress equation (e.g., Osman and Thorne, 1988; Langendoen and Simon, 2008):

$$\varepsilon_L = k\left(\frac{\tau}{\tau_c} - 1\right) \quad (6)$$

where $\varepsilon_L$ = lateral erosion rate (m s$^{-1}$), k = erodibility (m s$^{-1}$), $\tau$ = bed shear stress (Pa), and $\tau_c$ = critical shear stress (Pa). This equation was first used in studies of cohesive streambed and estuarine mud erosion (Partheniades, 1965; Ariathurai and Arulanandan, 1978). The volume of material eroded from each layer of the bank is converted to a concentration by size class and then added to the stream for transport by the 2D mobile-bed model.

2.3.3. Basal removal of failed bank materials

Large chunks of soil, or blocks, are often deposited at the bank toe following mass failure. These blocks temporarily protect the bank from direct fluvial erosion, but over time are subject to subaerial weathering (when exposed) and gradual winnowing and eventual removal (when submerged). Some previous researchers (e.g., Pizzuto, 1990; Nagata et al., 2000) assumed that after failure the fraction of failed material > 0.062 mm settles at the angle of repose in an area of variable width, computed to ensure conservation of mass. Others such as Darby and Delbono (2002) assumed that failed material settles at a specified angle (e.g., of 35°), approximating the mean angle of repose, but the lateral extent of the deposit was limited to a one-bank-height-wide region at the toe of the bank. This caused issues regarding mass conservation, and thus Darby et al. (2002) changed their formulation to permit the angle of the deposit to vary in order to ensure conservation of mass. However, Darby et al. (2002) also assumed that failed material > 10 mm in size immediately became bed material, with the grain size characteristics of the bed, and thus did not conserve mass within each grain size class. While these assumptions may be valid for a few isolated cases, imposing them upon all failures is unsafe under all flow conditions. More recent discussion of the protecting features of the failed blocks may be found in Darby et al. (2010) and Parker et al. (2011). In this study, we incorporate the basal removal process by placing failed bank materials into an invisible 'tank', with no topographic expression, that is made available for preferential scour by hydraulic fluvial erosion following mass failure (Langendoen, 2000). That is, the basal erosion process must erode the sediment within each size class in the tank before we permit erosion of material in that size class from the wetted bank face. The tank approach explicitly accounts for the protection afforded by failed bank materials, conserves the mass, and does not require us to make assumptions regarding the topographic form of failed blocks. The treatment ignores the impact of block geometry on near-bank flows simulated by the 2D model. We further assume that weathering does not change the erosion resistance of the failed materials, and the establishment and proliferation of vegetation in the near-bank zone are not taken into consideration.

2.3.4. Mesh strategy

A key remaining issue within the coupling procedure is how to simulate the feedbacks between the morphological changes predicted by the bank model and those predicted by the 2D mobile-bed model. We can tackle this issue using either a fixed mesh approach or a moving mesh approach.

The fixed mesh approach does not move the mesh in planform in response to bank retreat, and thus it does not need additional interpolations. However, streambanks do not always align with mesh lines, and thus bank retreat cannot be represented accurately using nearby in-channel mesh nodes. Therefore, unless we employ a highly refined mesh, accuracy is seriously in question. Use of such a refined mesh significantly increases computational cost. In contrast, the moving mesh approach maintains the mesh size and connectivity and dynamically moves mesh lines to align them with the streambank throughout the simulation period. Therefore, the moving mesh approach accurately represents bank retreat. The added computation is that the mesh has to be ‘moved’ every time the bank retreats; but the computational cost is very low in comparison with the fixed mesh approach. Herein, the Arbitrary Lagrangian-Eulerian (ALE) formulation of Lai and Przekwas (1994) is adopted. This formulation arbitrarily moves the mesh using the governing equations expressed in integral form:

$$\frac{d}{dt}\int_A h\,dA + \int_S h(\vec{V}-\vec{V}_g)\bullet d\vec{S} = 0 \qquad (7a)$$

$$\frac{d}{dt}\int_A h\vec{V}\,dA + \int_S h\vec{V}(\vec{V}-\vec{V}_g)\bullet d\vec{S} = \int_S h\vec{\vec{\sigma}}\bullet d\vec{S} + \int_A \vec{S}_V\,dA \qquad (7b)$$

$$\frac{d}{dt}\int_A h\phi\,dA + \int_S h\phi(\vec{V}-\vec{V}_g)\bullet d\vec{S} = \int_S h\vec{q}\bullet d\vec{S} + \int_A S_s\,dA \qquad (7c)$$

In the above, Eq. (7a) is the mass conservation, Eq. (7b) is the momentum conservation, Eq. (7c) is for transport of any scalars (e.g., sediment concentration for each size class), t = time (s), h = flow depth (m), A = area of an arbitrary mesh cell (m$^2$), $\vec{S}$ = the side length of the cell (m) with arrow representing the unit normal, $\vec{V}$ = the fluid flow velocity vector (m s$^{-1}$), $\vec{V}_g$ = the velocity vector of the moving mesh (m s$^{-1}$), $\vec{\vec{\sigma}}$ = the stress tensor owing to dispersion (m$^2$s$^{-2}$), and $\vec{S}_V$ and $S_S$ represent the source terms of each equation. Note that the second terms on the left hand side introduce an extra unknown, the mesh velocity $\vec{V}_g$, owing to mesh movement. The mesh velocity is computed using a geometric constraint called space conservation written as:

$$\frac{d}{dt}\int_A dA = \int_S \vec{V}_g \bullet d\vec{s} \qquad (8)$$

A special procedure was developed by Lai and Przekwas (1994) to enforce equation (8) in such a way that the computed grid velocity conserves mass exactly. Once $\vec{V}_g$ is computed, the discretization and solution algorithms are the same as the fixed mesh case. With the current ALE method, the main flow and sediment variables represented by the mesh cell are automatically computed in a time-accurate manner and there is no need for additional interpolations.

Remeshing is needed after bank retreats. In this study, the spring analogy is used to redistribute all mesh points automatically. That is, the following equation is solved at each mesh node i:

$$\sum_{\mathrm{all-edges}}\left\{k_f\left(\vec{\delta}_f-\vec{\delta}_i\right)\right\}=0 \qquad (9)$$

where the summation is over all edges connected to node i, and f is the node connected to i at the other end of the edge, $\vec{\delta}_f$ and $\vec{\delta}_i$ are the distance vector of the nodal movement of f and i, respectively, and $k_f$ is the stiffness of the edge that is taken as the inverse of the edge length. After mesh movement, bed topography is updated using linear interpolation.

2.3.5. Model execution: information flow

The time scale of the bank retreat process is much longer than that of instream hydraulic and sediment transport processes, and thus the time step of the bank retreat submodel is generally much longer than the 2D mobile-bed model. During a typical simulation, the model first fixes the positions of the banks, and then simulates 2D flow, sediment transport, and vertical bed deformation first. The mobile-bed simulation continues in this manner until the time step of the bank retreat submodel is reached. The model then

(1) time-averages the near-bank values of the shear stress and water elevation over the duration of the bank retreat time step;
(2) vertically distributes the near-bank shear stress;
(3) computes the amount of material eroded from the tank;
(4) computes the amount of lateral (fluvial) erosion of the bank face (if any) and deforms the bank section accordingly; and
(5) computes the geotechnical stability of the bank and updates the geometry of the bank section accordingly.

After the bank model completes its bank retreat modeling, the predicted distances of bank toe and bank top retreat are used to move the mesh lines and the 2D mesh is redistributed; any material removed by fluvial processes from the banks is added to the stream for transport by the 2D model; any material from geotechnical failures is added to the tank to protect the bank toe. Thus, while the model is a fully coupled 2D flow, sediment transport, and bank retreat model, it does so in a decoupled manner (Kassem and Chaudhry, 1998).

## 3. Model verification

The flow and sediment model SRH-2D has been extensively verified in our previous publications (e.g., Lai, 2008, 2010, 2011; Lai and Greimann, 2008, 2010; Lai et al., 2011). The coupled bank stability and 2D mobile-bed model reported herein has also been tested and verified (see our project report, Lai et al., 2012). Herein an extra verification case is simulated to ensure that the moving mesh ALE algorithm of Lai and Przekwas (1994) has been implemented correctly; in the process, the consequence of not using it is also discussed.

An open channel flow through a 10-m-long by 2-m-wide straight channel is set up and simulated with SRH-2D; the flow discharge is 3.0 $m^3s^{-1}$. Constant longitudinal velocity of 1.21 $ms^{-1}$ and zero lateral velocity should be the exact solution if the flow is frictionless and the two side boundaries are set to be symmetry. First, it is verified that the exact solution is obtained with SRH-2D using either the mesh displayed in Fig. 3a or Fig. 3b. Next, an unsteady simulation is carried out for the same flow, but allowing the mesh to change from Fig. 3a to Fig. 3b in one second. When the ALE moving formulation developed in this study is activated, the predicted velocities are found to remain exactly the same. This test verifies that the ALE method has been implemented correctly in our model as flow velocities should not be disturbed by mesh movement. Further, we carry out a simulation by turning off the moving mesh algorithm while the mesh is moving in order to shed light on the consequence of not adopting the moving mesh formulation. The predicted velocity is found to be disturbed, with lateral velocity being as much as 0.012 $ms^{-1}$ instead of zero (see the lateral velocity contours in Fig. 3c), and longitudinal velocity varying between 1.192 and 1.234 $ms^{-1}$ (a 3.4% change). This simple case shows that erroneous results may be produced if a mesh is moved owing to bank retreat, but mesh movement is not taken into consideration.

## 4. Model validation

A field case is presented to validate the coupled model, demonstrate its use and some of its features, and draw key conclusions. We use the model to simulate the morphodynamics of a bend on Goodwin Creek, Mississippi, for the period between March 1996 and March 2001. We selected this site because of the wealth of data available from a long-term streambank failure monitoring study carried out since 1996. Bank retreat data, as well as other hydrological and geotechnical data, are available over a six-year period, making the site ideal for testing the coupled model. The morphology and dynamics of the study site were described and discussed by Grissinger and Murphey (1983), Simon et al. (2000), and Langendoen and Simon (2008). In addition, the bend was numerically simulated with a coupled 1D flow, sediment transport, and bank stability model (CONCEPTS) by Langendoen and Simon (2008). The present study may thus also shed light on whether the use of a 2D mobile-bed model has advantages over a 1D model.

### 4.1. Model setup

Inputs and modeling steps for the coupled bank stability and 2D model remain the same as for conventional mobile-bed modeling. That is, we develop an initial solution domain with a 2D mesh to represent the initial channel topography and specify boundary conditions. The only change for coupled modeling is to identify retreating bank positions on the 2D mesh. All retreating banks are grouped into a number of bank segments, and each segment is defined on the

2D mesh by two mesh lines. The first defines the bank toe, while the second defines the bank top. The two form a mesh polygon that represents the retreating bank segment, called a bank zone in this paper. Fig. 4 shows the solution domain and the mesh used for the Goodwin Creek modeling in which the outer red box on the right bank is the selected bank zone.

A separate input file is prepared for the bank erosion model. First, an arbitrary number of bank profiles are selected to represent retreating bank segments (bank segment discretization), and bank retreat between two profiles is obtained through linear interpolation. Input parameters are then given profile by profile. For each bank profile, an arbitrary number of nodes may be used to define the bank geometry, which is independent of the 2D mesh, as long as the toe and top nodes coincide with those on the 2D mesh. This way, the bank retreat model may use many more points on the bank face than the 2D mesh allows. The dual representation of banks ensures that fluvial erosion and geotechnical stability analysis may be accurately simulated. In the Goodwin Creek modeling, 11 bank profiles are selected (see Fig. 4). Further, the number of 2D mesh points in the primary flow direction, longitudinal, is also unrelated to the number of bank profiles and is usually much larger than the number of bank profiles. For our example, the longitudinal mesh nodes have seven times more than the number of bank profiles. The input parameters for each bank profile include: (i) groundwater elevation, (ii) bank stratigraphy (layering information); (iii) critical shear stress and erodibility of each layer; (iv) geotechnical properties of each layer, such as effective cohesion and effective angle of internal friction; and (v) sediment composition of each layer.

The initial stream and bank topography was developed from a survey of 11 cross sections carried out in March 1996 (see the survey points and the resultant bathymetry in Fig. 4); the solution domain and initial 2D mesh, along with the bank zone, are also shown in Fig. 4. We selected 11 bank profiles on the right bank, corresponding to the 11 surveyed cross sections, for bank retreat simulation. This compares to 71 2D mesh points in the streamwise direction. Conversely, we used 9 to 16 surveyed points to represent the geometry of the bank face between the toe and the bank top, while we used only 6 lateral 2D mesh points for each profile. Mesh sensitivity analysis showed that the mesh is adequate for the study.

The inputs for the flow and sediment transport components of the coupled model were:

(1) The recorded time series discharge was applied at the upstream boundary (XS-1) (Fig. 5a). Sediment transport rate computed by the equation of Wilcock and Crowe (2003) was imposed at the upstream boundary.

(2) The stage-discharge rating curve was developed from coincident stage and discharge records measured in 2001, and it was enforced at the downstream boundary (XS-11). The resulting stage at XS-11 is displayed in Fig. 5b.

(3) Table 1 lists the grain size composition of the bed material, segregated into the nine size classes used by SRH-2D. The bed material of Goodwin Creek is bimodal with peaks at 0.5 and 22.6 mm, a median grain size of 6.7 mm, and a gradation coefficient of 8.2 (Langendoen and Simon, 2008). The transport of each size class was governed by its own differential transport equation that used the Wilcock and Crowe (2003) equation to compute the sediment pickup potential.

(4) A constant Manning's roughness coefficient of 0.032 was used within the main channel; it was estimated using coincident discharge and stage records measured at the upstream and downstream boundaries in 2001.

The inputs for the bank retreat components of the coupled model were mostly from the survey data and they were:

(1) At XS-1, the bank was composed of a single cohesive layer with the measured properties of effective cohesion, $c' = 4.5$ kPa; effective friction angle, $\phi' = 28.6°$; angle describing the increase in shear strength for an increase in matric suction, $\phi^b = 10.4°$; saturated unit weight, $\gamma_s = 19.4$ kN m$^{-3}$; and porosity = 0.38.

(2) At XS-2 to XS-11, the bank was composed of four layers, and all properties were similar to that measured at XS-6 based on the data in March 1996 (see Fig. 6). Table 2 lists the geotechnical properties measured while TableTable 1 lists the sediment composition of each layer in the bank, segregated into the nine size classes used for sediment transport modeling. These properties closely followed those presented by Simon et al. (2000) and were taken from those used by Langendoen and Simon (2008).

(3) We assigned a critical shear stress of 5.35 Pa to all bank profiles. This value represents the median of 16 nonvertical and vertical jet tests (Hanson, 1990; Hanson and Simon, 2001) conducted on failed bank materials at the study site (16$^{th}$ and 84$^{th}$ percentiles were 0.17 and 24.6 Pa, respectively). This is different from the approach taken by the 1D modeling of Langendoen and Simon (2008) who took the critical shear stress as a calibration parameter and allowed it to vary at different cross sections throughout the bend. A single parameter along the entire bend simplifies data collection needs for field application of the model.

(4) We assumed that the groundwater elevation was constant at 82.3 m throughout the simulation. This approximates the top of a less permeable soil layer containing manganese nodules (Simon et al., 2000; Cancienne et al., 2008). In addition, tensiometric pore-water pressure data collected at the study site between 1997 and

2004 by the USDA-ARS (see Simon and Collison, 2002, for a subset of this data set) indicated that the elevation of the groundwater table varied from between ~ 81.3 m and 82.3 m. We note that the assumption of a constant groundwater table elevation is very simplistic and its impact is to be discussed later in the paper.

No calibration of the above geotechnical properties of the bank was attempted in this study to improve the similarity between the predictions of the model and the measured data because too many calibration parameters will complicate the practical usefulness of the model. The erodibility k (see Eq. 6) is the only parameter that remains to be specified. Three methodologies are possible to inform its selection. First, the submerged jet test produced an estimate of k as part of the least-square fitting procedure to estimate $\tau_c$ (Hanson, 1990; Hanson and Simon, 2001). Second, Arulanandan et al. (1980) and Hanson and Simon (2001) published empirical equations relating k to $\tau_c$. Third, k is used simply as a calibration parameter. We recommend the third approach, i.e., erodibility is calibrated but the same value should be used for all bank profiles within a bank segment having similar properties. For our Goodwin Creek case, a single value for erodibility is to be calibrated. Reasons for this recommendation are multiple. First, measured erodibility is usually subject to order-of-magnitude uncertainty in the field. Second, only one set of geotechnical field measurements are usually carried out at a single location that is assumed to represent the average properties of a larger bank segment. Allowing variation of the erodibility over a bank segment will complicate the model and make the calibration process impractical. Further, the calibration approach offers the potential to take into consideration other factors that influence bank erosion, such as soil conditions and covers such as vegetation. As a matter of fact, our approach takes erodibility as the only major calibration parameter, while it leaves others from surveyed or estimated data. Jet-testing carried out at Goodwin Creek yielded a median k of

$1.47 \times 10^{-6}$ m $s^{-1}$, with $10^{th}$ and $90^{th}$ percentiles of $1.18 \times 10^{-7}$ and $3.74 \times 10^{-6}$ m $s^{-1}$, respectively. In this study, the calibrated value of k was $1.2 \times 10^{-7}$ $ms^{-1}$. The calibrated value is close to the $10^{th}$ percentile of the measured range. The most likely explanation is the change of material properties caused by the subaerial drying, hardening, and compaction. It may also reflect the impact of vegetation growth on the bank toe.

The time step of the 2D model was 5 seconds, while the time step of the bank model was variable and was the time needed for a given amount of water flowing through the bend. In the simulation, a volume of 4000 $m^3$ was used to compute the time step of the bank model. Sensitivity analysis indicated that model results are insensitive to further reduction of these time steps.

### 4.2. Model results

#### 4.2.1. Morphological change

The predicted bank retreat from March 1996 to March 2001 is compared with measured data in Fig. 7. The initial and final 2D meshes are plotted in Fig. 8. A more detailed comparison between the predicted results and measured data are made in Fig. 9, in which bank retreat processes are shown for selected banks at different times. Further, the predicted and observed net bank retreat distance is compared in Fig. 10.

These results show that the overall agreement between the model prediction and the survey data is good, considering that the site is quite complex with many physical processes involved (see discussion below). A more quantitative comparison is made in Table 3, which displays predicted and observed channel top widths for cross sections 4 to 9 at the Goodwin Creek site in March 2001 (see also a similar comparison by Langendoen and Simon, 2008, with the 1D model). The change in channel top width is an indicator of the loss of land adjacent to the stream caused by bank erosion. The average top width is slightly overpredicted by 0.66 m, with a relative error of 2.2%. The simulated average bank retreat distance along the bendway (3.68 m) is slightly larger than the observed (3.33 m) (Fig. 10). The difference between the predicted and observed top width ranges from 0.2% to 5.2% between cross sections 4 to 9. A planform view of the changes may be seen in Fig. 7.

Despite the overall success, however, several areas need attention. First, the location of the tension crack (vertical bank lines from the bank top) is not predicted well at some cross sections. At cross sections 5 and 9, for example, the tension crack is predicted to be too far away from the bank in earlier years, relative to the observed data. A large volume of bank material is predicted to fail very early and become available to protect the bank toe. This makes the bank profile remain relatively stable for a long period of time, as these materials have to be removed by fluvial erosion. The tension crack algorithm is also found to be sensitive to several model input parameters and is an area that needs future research. Second, the timing and volume of mass failures are not always in agreement with the observed data at some locations. This poor prediction is partly owing to the tension crack algorithm mentioned above, but is certainly attributed to other causes. One of them is probably the use of the simple basal cleanout model. Generally, the rate of erosion of the pre-failure bank and the failed materials are not the same, but this is the assumption used by the present cleanout model. Development of more accurate, yet still simple and practical, cleanout models is another area of future study. We suspect that a more probable cause of timing mismatch may be the simple groundwater table assumption (horizontal and constant) presently employed and therefore, we next explore model sensitivity to water table elevation.

4.2.2. Sensitivity to groundwater elevation

Poor prediction of bank failure timing is probably caused by the impact of a perched water table during rainfall events as pointed out by Langendoen and Simon (2008). The study site is greatly influenced by rainfall. The loss of matric suction from infiltrating precipitation and subsequent seepage is important in contributing to mass failure. Langendoen and Simon (2008) observed that large losses of matric suction in the upper part of the bank are common at the site in response to storms with only a moderate amount of rainfall (about 25 mm). This leads to more frequent, smaller failures of the upper part of the bank. To see how bank retreat responds to water table variation, we carried out a sensitivity analysis with two additional model runs in which groundwater table elevation was set at 81.3 and 83.3 m, respectively. The predicted bank retreat distances are compared with the observed and with the 82.3 m data in Fig. 10. As expected, lowered groundwater table elevation reduces the retreat distance, while heightened groundwater table elevation increases retreat distance. We see that bank retreat is relatively sensitive to water table elevation. Average retreat distance along the bendway is predicted to vary by 43% when water table elevation is reduced from 83.3 to 81.3 m. The present model assumed that the water table elevation was constant over the simulation period, which, therefore, was probably responsible for the inaccurate prediction of failure timing at some locations. This analysis suggests that another avenue for future research is to incorporate a model of water table motion caused by rainfall events and/or seepage, such as the attempt made by Langendoen (2010).

Nevertheless, despite the timing issues discussed above, the present study shows that even at a complex site like Goodwin Creek the model can predict bank retreat relatively reliably over an annual or multiyear hydrograph. In simulations with a constant groundwater table elevation, the overall retreat integrated over the modeling period is sought, not the details of short-term bank failure timing. Accurate event-based bank erosion modeling will likely only be possible with the incorporation of a more sophisticated model of water table motion.

4.2.3. Discussion

Bank erosion modeling at Goodwin Creek is very challenging as the banks are tall and steep, consist of multilayer cohesive materials, and are impacted by positive and negative pore-water pressures and seepage. In addition, the structure of the massive silt and meander belt alluvium units promotes the development of large vertical tension cracks (Grissinger and Murphey, 1983) that seem to dominate the shape of the bank profile. Despite these complexities, the present coupled model has been able to reproduce the bank retreat process as well as the formation of the new bank shape with tension cracks. Overall, the predicted results agree reasonably with the measured data over the five-year simulation period.

More importantly, the primary objective of the present study is to develop a new framework and the associated algorithms that integrate bank erosion and 2D mobile-bed submodels within a flexible, robust, and easy-to-apply model. The validation study of the Goodwin Creek bendway shows that our proposed framework and coupling procedure work well; the model is easy to set up and the numerical procedures maintain numerical stability and improve accuracy. The study also allows us to recommend a calibration procedure that is simple to apply in the field: erodibility is selected as a single calibration parameter for each bend or along a bank segment with similar bank materials. Using the erodibility as a calibration parameter allows the incorporation of more subtle erosion processes that are not modeled explicitly, such as seepage and vegetation, into simulations.

Although different critical shear stress and erodibility coefficient values were used for different cross sections by Langendoen and Simon (2008), we used the same values at all cross sections. Langendoen and Simon (2008) reported calibrated critical shear stress values of (in Pa): 8, 8, 4, 4, 2, 1, 1, 1, 4, 8, 8, respectively, from cross section 1 through 11. The predicted bank retreat distance by Langendoen and Simon (2008) is also included in Table 3 for comparison. The average top width predicted by CONCEPTS is about 1.7% smaller than the observed, while the present model is 2.2% more. Similar results are predicted with the present 2D model in comparison with CONCEPTS. This demonstrates that the use of a 2D mobile-bed model for the main channel is more advantageous than a 1D modeling approach as fewer calibration parameters are needed with our 2D model. We used only one value of erodibility along the bendway, while Langendoen and Simon (2008) applied different values at different bank cross sections. In general, 1D models cannot predict the enhanced near-bank shear stress at a bend. A reduction of the critical shear stress at some cross sections was probably a calibration effort to match the measured data. The present coupled bank stability and 2D mobile-bed model holds better potential to be applicable to the field since determination of calibration parameters can be reach-based rather than individual cross section based.

## 5. Concluding remarks

A fully coupled flow, sediment transport, and bank stability model to predict bank retreat in alluvial streams has been developed in this study. Our major contribution is the development of a general framework and the associated numerical procedure that allow a seamless integration of a popular mechanistic bank erosion model (BSTEM) and a widely used 2D mobile-bed model (SRH-2D). The bank stability model handles the mechanistic basal erosion and mass failure of a bank, while the 2D model simulates the fluvial processes near the bank toe and in the stream. To our knowledge, our study is among the first to accomplish complete coupling of a multilayer cohesive bank model and a multidimensional mobile-bed model and to demonstrate its application in a dynamic, continuous, geofluvial simulation. Our new model overcomes a number of limitations of previous models, and the coupling procedure is demonstrated to maintain solution robustness and accuracy while remaining user friendly.

The coupled model has been validated by applying it to Goodwin Creek bendway in Mississippi over a simulation period of five years. Comparisons among the predicted and observed data, as well as the results of a previous 1D modeling study, show that our model can replicate bank retreat and its shape over the 5-year period. The study also shows that the use of the 2D mobile-bed model SRH-2D leads to improvements over that of the 1D model in that only a single calibration parameter is needed to obtain reasonable erosion estimates for the entire bendway. The simpler calibration process means our new model may be used as a practical tool to predict planform changes of streams. Some practical applications have already been conducted and reported (see Lai, 2014).

However, this study also highlights a few avenues for future research, related mostly to the applicability and accuracy of some submodels. The objective of the present work was to set up a general framework for the coupled model in order to address existing model limitations; in the process, all five identified modeling elements were incorporated. With the developed general framework, we believe the opportunity is now ripe to incorporate more accurate submodels into the coupled model. First, an improved approach to estimate maximum tension crack depth is needed. Second, more general yet still simple and practical basal cleanout algorithms may be needed as our simple tank model may lead to incorrect prediction of the timing of fluvial erosion and hence bank failures. The extra form roughness and local flow modifications by the failed blocks may already be taken into consideration by the present model. Third and perhaps most importantly, we adopted the simplistic assumption of a constant elevation, horizontal groundwater table. As groundwater table gradients and movements are important for seepage and bank failure (Rinaldi and Nardi, 2013), this is likely to have contributed to incorrect predictions of the timing of mass failure and will continue to limit our coupled model to the prediction of multiyear average bank retreat. Future improvement thus requires the incorporation of groundwater elevation variation into the model so that storm event-based bank erosion may be simulated. Finally, our model is limited to bank erosion modeling only; so it cannot be used to predict channel planform development as bank accretion is not included. Modeling of bank accretion is another area of future research so that channel meandering processes may also be simulated.

**Acknowledgements**

This study was sponsored by the Science and Technology Program of Reclamation and the Water Resources Agency of Taiwan. The project Liaison Officer, Director Hung-Kwai Chen, and the review committee in Taiwan provided valuable technical comments. Much of the code within the bank stability submodel was inspired by the work of Eddy Langendoen of the USDA-ARS National Sedimentation Laboratory, Oxford, MS. The second author is grateful to Dr. Langendoen for providing code snippets as well as extremely fruitful conversations and discussions. The editor and anonymous reviewers have offered suggestions which have greatly improved the presentation of this research.

## References

Ariathurai, R., Arulanandan, K., 1978. Erosion rates of cohesive soils. Journal of the Hydraulics Division, ASCE, 104(HY2), 279–283.

Arulanandan, K., Gillogley, E., Tully, R., 1980. Development of a quantitative method to predict critical shear stress and rate of erosion of natural undisturbed cohesive soils. Technical Report GL-80-5. U.S. Army Engineers Waterways Experiment Station: Vicksburg, MS.

ASCE Task Committee on Hydraulics, Bank Mechanics and Modeling of River Width Adjustment, 1998. River width adjustment II: Modeling. J. Hydraulic Engineering, ASCE, 124(9), 903–917.

Cancienne, R.M, Fox, G., Simon, A., 2008. Influence of seepage undercutting on the stability of root-reinforced streambanks. Earth Surface Processes and Landforms, 33(11), 1769–1786.

Chang, H.H., 1979. Minimum stream power and river channel patterns. Journal of Hydrology, 41, 301–327.

Chen, D., Duan, J.G., 2006. Modeling width adjustment in meandering channels. Journal of Hydrology, 321, 59–76.

Darby, S.E., Delbono, I., 2002. A model of equilibrium bed topography for meander bends with erodible banks. Earth Surface Process and Landforms, 27(10), 1057–1085.

Darby, S.E, Thorne, C.R., 1996a. Numerical simulation of widening and bed deformation of straight sand-bed rivers, I: Model development. J. Hydraulic Engineering, ASCE, 122, 184–193.

Darby, S.E, Thorne, C.R., 1996b. Stability analysis for steep, eroding, cohesive riverbanks. J. Hydraulic Engineering, ASCE, 122, 443–454.

Darby, S.E., Gessler, D., Thorne, C.R., 2000. Computer program for stability analysis of steep, cohesive riverbanks. Earth Surface Process and Landforms, 25(2), 175–190.

Darby, S.E., Alabyan, A.M, van de Wiel, M.J., 2002. Numerical simulation of bank erosion and channel migration in meandering rivers. Water Resources Research, 38, 1163–83.

Darby, S.E., Rinaldi, M., Dapporto, S., 2007. Coupled simulations of fluvial erosion and mass wasting for cohesive river banks. Journal of Geophysical Research, 112(F03022), 1–15. (doi:10.1029/2006JF000722).

Darby, S. E., Trieu, H.Q., Carling, P.A., Sarkkula, J., Koponen, J., Kummu, M., Conlan, I., Leyland, J., 2010. A physically based model to predict hydraulic erosion of fine-grained riverbanks: The role of form roughness in limiting erosion, J. Geophys. Res., 115, F04003, doi:10.1029/2010JF001708

de Cacqueray, N., Hargreaves, D.M., Morvan, H.P., 2009. A computational study of shear stress in smooth rectangular channels. J. Hydraulic Research, 47(1), 50–57

Duan, G., Wang, S.S.Y., Jia, Y., 2001. The applications of the enhanced CCHE2D model to study the alluvial channel migration processes. J. Hydraulic Research, 39, 469–480.

Dunne, T., Leopold, L.B., 1978. Water in environmental planning. W.H. Freeman, San Francisco, 818 pp.

Eaton, B.C., 2006. Bank stability analysis for regime models of vegetated gravel bed rivers. Earth Surface Processes and Landforms 31(11): 1438-1444.

Einstein, H.A., 1942. Formulas for the transportation of bed load. Transactions of the ASCE, 107, 561–597.

Environment Agency, 1999. Waterway bank protection: a guide to erosion assessment and management; R and D Publication 11. Environment Agency, Bristol, UK, 235 pp.

Florsheim, J.L., Mount, J.F., Chin, A., 2008. Bank erosion as a desirable attribute of rivers. BioScience, 58(6), 519–529.

Fredlund, D.G., Rahardjo, H., 1993. Soil Mechanics of Unsaturated Soils. John Wiley and Sons, Inc., New York, NY.

Fredlund, D.G., Morgenstern, N.R., Widger, R.A., 1978. The shear strength of unsaturated soils. Canadian Geotechnical Journal, 15, 313–321.

GEO-SLOPE International, 2008. Stability modeling with SLOPE/W 2007 Version: An Engineering Methodology, 4th Ed. GEO-SLOPE International, Calgary, Canada.

Greimann, B.P., Lai, Y.G., Huang, J., 2008. Two-dimensional total sediment load model equations. J. Hydraulic Engineering, ASCE, 134(8), 1142–1146.

Grissinger, E.H., Murphey, J.B., 1983. Present channel stability and late quaternary valley deposits in northern Mississippi. In: Collinson, J.D., Lewin, J. (Eds.), Modern and Ancient Fluvial Systems, Blackwell Scientific Publications, Oxford, UK, 241–250.

Guo, J., Julien, P.Y., 2005. Shear stress in smooth rectangular open-channel flows. J. Hydraulic Engineering, ASCE, 131(1), 30–37.

Hanson, G.J., 1990. Surface erodibility of earthen channels at high stress, Part II - Developing an in situ testing device. Transactions of the American Society of Agricultural Engineers, 33(1), 132–137.

Hanson, G.J., Simon, A., 2001. Erodibility of cohesive streambeds in the loess area of the midwestern USA. Hydrological Processes, 15(1), 23–38.

Hasegawa, K., 1977. Computer simulation of the gradual migration of meandering channels. Proceedings of the Hokkaido Branch. Japan Society of Civil Engineering, pp. 197–202 (in Japanese).

Hasegawa, K., 1981. Bank-erosion discharge based on a nonequilibrium theory. Proceedings of Japan Society of Civil Engineering, Tokyo, 316, 37–50 (in Japanese).

Hey, R.D., Thorne, C.R., 1986. Stable channels with mobile gravel beds. Journal of the Hydraulics Division, ASCE, 112, 671–689.

Howard, A., Raine, S.R., Titmarsh, G., 1998. The contribution of stream bank erosion to sediment loads in Gowrie Creek, Toowoomba. ASSI National Soils Conference, Brisbane, vol. 2004, pp.491–493.

Huang, H.Q., Nanson, G.C., 2000. Hydraulic geometry and maximum flow efficiency as products of the principle of least action. Earth Surface Processes and Landforms, 25, 1–16.

Huang, Y.H., 1983. Stability analysis of earth slopes. Van Nostrand Reinhold Company, New York.

Ikeda, S., Parker, G., Sawai, K., 1981. Bend theory of river meanders. Part I. Linear development. Journal of Fluid Mechanics, 112, 363–377.

Kassem, A.A., Chaudhry, M.H., 1998. Comparison of coupled and semicoupled numerical models for alluvial channels. J. Hydraulic Engineering, ASCE, 124(8), 794–802.

Kean, J.W., Smith, J.D., 2006a. Form drag in rivers due to small-scale natural topographic features: 1. Regular sequences. Journal of Geophysical Research, 111(F04009). DOI: 10.1029/2006JF000467.

Kean, J.W., Smith, J.D., 2006b. Form drag in rivers due to small-scale natural topographic features: 2. Irregular sequences. Journal of Geophysical Research, 111(F04010). DOI: 10.1029/2006JF000490.

Kean, J.W., Kuhnle, R.A., Smith, J.D., Alonso, C.V., Langendoen, E.J., 2009. Test of a method to calculate near-bank velocity and boundary shear stress. J. Hydraulic Engineering, ASCE, 135(7), 588–601.

Khodashenas, S.R., El Kadi Abderrezzak K., Paquier, A., 2008. Boundary shear stress in open channel flow: A comparison among six methods. J. Hydraulic Research, 46(5), 598–609.

Kirkby, M.J., 1977. Maximum sediment efficiency as a criterion for alluvial channels. In: Gregory, K.J. (Ed.), River Channel Changes. Wiley, Chichester, pp. 429–442.

Lai, Y.G., 2008. SRH-2D Theory and User's Manual version 2.0, Technical Service Center, Bureau of Reclamation, Denver, CO.

Lai, Y.G., 2010. Two-dimensional depth-averaged flow modeling with an unstructured hybrid mesh. J. Hydraulic Engineering, ASCE, 136(1), 12–23.

Lai, Y.G., 2011. Prediction of channel morphology upstream of Elephant Butte Reservoir on the middle Rio Grande. Report SRH-2011-04, Technical Service Center, Bureau of Reclamation, Denver, CO.

Lai, Y.G., 2014. Advances in Geofluvial Modeling: Methodologies and Applications. Chapter 6 in Advances in Water Resources Engineering, C.T. Yang and L. K. Wang (eds), Humana Press, Springer Science and Business Media, to appear.

Lai, Y.G., Greimann, B.P., 2008. Modeling of erosion and deposition at meandering channels. World Environmental & Water Resources Congress, May 12-16, Honolulu, Hawaii.

Lai, Y.G., Greimann, B.P., 2010. Predicting contraction scour with a two-dimensional depth-averaged model. J. Hydraulic Research, 48(3), 383–387.

Lai, Y.G., Przekwas, A.J., 1994. A finite-volume method for fluid flow simulations with moving boundaries. Computational Fluid Dynamics, 2, 19–40.

Lai, Y.G., Weber, L.J., Patel, V.C., 2003. Non-hydrostatic three-dimensional method for hydraulic flow simulation, Part I: formulation and verification. J. Hydraulic Engineering, ASCE, 129(3), 196–205.

Lai, Y.G., Greimann, B.P., Wu, K., 2011. Soft bedrock erosion modeling with a two dimensional depth-averaged model. J. Hydraulic Engineering, ASCE, 137(8), 804–814.

Lai, Y.G., Greimann, B.P., Simon, A., 2012. A coupled stream bank erosion and two-dimensional mobile-bed model, SRH-2013-04, Technical Service Center, Bureau of Reclamation, Denver, CO.

Langendoen, E.J., 2000. CONCEPTS – Conservational channel evolution and pollutant transport system. Research Report 16, USDA Agricultural Research Service National Sedimentation Laboratory, Oxford, MS.

Langendoen, E.J., 2010. Assessing post-dam removal sediment dynamics using the CONCEPTS computer model. In: Proceedings of the 2nd Joint Federal Interagency Conference, Las Vegas, NV, June 27-July 1, 2010, 12 p.

Langendoen, E.J., Simon, A., 2008. Modeling the evolution of incised streams. II: Streambank erosion. J. Hydraulic Engineering, ASCE, 134(7), 905–915.

Langendoen, E.J., Wells, R.R., Thomas, R.E., Simon, A., Bingner, R.L., 2009. Modeling the evolution of incised streams. III: model application. J. Hydraulic Engineering, 135(6), 476–486.

Leopold, L.B., Maddock, T., 1953. The hydraulic geometry of stream channels and some physiographic implications. US Geological Survey Professional Paper 252, US Geological Survey. 57pp.

Luppi, L., Rinaldi, M., Teruggi, L.B., Darby, S.E., Nardi, L., 2009. Monitoring and numerical modelling of riverbank erosion processes: A case study along the Cecina River (central Italy). Earth Surface Processes and Landforms, 34(4), 530–546.

Morgenstern, N.R., Price, V.R., 1965. The analysis of the stability of general slip surfaces. Geotechnique, 15, 79–93.

Mosselman, E., 1998. Morphological modeling of rivers with erodible banks. Hydrological Processes, 12, 1357–1370.

Motta, D., Abad, J.D., Langendoen, E.J., Garcia, M.H., 2012. A simplified 2D model for meander migration with physically-based bank evolution. Geomorphology, 163-164, 10–25.

Nagata, N., Hosoda, T., Muramoto, Y., 2000. Numerical analysis of river channel processes with bank erosion. J. Hydraulic Engineering, ASCE, 126(4), 243–252.

Osman, M.A., Thorne, C.R., 1988. Riverbank stability analysis: I. Theory. J. Hydraulic Engineering, ASCE, 114(2): 134–150.
Parker, G., Shimizu, Y., Wilkerson, G. V., Eke, E. C., Abad, J. D., Lauer, J. W., Paola, C., Dietrich, W. E. and Voller, V. R., 2011. A new framework for modeling the migration of meandering rivers. Earth Surf. Process. Landforms, 36: 70–86. doi: 10.1002/esp.2113.
Partheniades, E., 1965. Erosion and deposition of cohesive soils. Journal of Hydraulics Division, ASCE, 91(HY1), 105–139.
Piégay, H., Darby, S.E., Mosselman, E., Surian, N., 2005. A review of techniques available for delimiting the erodible river corridor: a sustainable approach to managing bank erosion. River Research and Applications, 21(7), 773-789.
Pizzuto, J.E., 1990. Numerical simulation of gravel river widening, Water Resources Research, 26, 1971–1980.
Pollen, N.L., Simon, A., 2005. Estimating the mechanical effects of riparian vegetation on stream bank stability using a fiber bundle model. Water Resources Research, 41(7), W0702510.1029/2004WR003801.
Pollen-Bankhead, N., Simon, A., 2009. Enhanced application of root-reinforcement algorithms for bank-stability modeling. Earth Surface Processes and Landforms, 34(4), 471–480.
Press, W.H., Teukolsky, S.A., Vetterling, W.T., Flannery, B.P., 1992. Numerical Recipes in Fortran: The Art of Scientific Computing, (2nd Ed.). Chichester, UK: John Wiley & Sons, Ltd., pp.404–405.
Rinaldi, M., Darby, S.E, 2008. Modelling river-bank-erosion processes and mass failure mechanisms: Progress towards fully coupled simulations. In: Habersack, H., Piégay, H., Rinaldi, M. (Eds), Gravel-Bed Rivers 6: From Process Understanding to River Restoration; Developments in Earth Surface Processes 11. Elsevier: Amsterdam; pp.213–239.
Rinaldi, M., Nardi, L., 2013. Modeling interactions between riverbank hydrology and mass failures. J. Hydrol. Eng., 18(10), 1231–1240.
Rinaldi, M., Mengoni, B., Luppi, L., Darby, S.E., Mosselman, E., 2008. Numerical simulation of hydrodynamics and bank erosion in a river bend. Water Resources Research, 44, (W09428) (doi:10.1029/2008WR007008).
Schumm, S.A., 1968. River adjustment to altered hydrologic regime – Murumbidgee River and Paleochannels, Australia. U.S. Geological Survey Professional Paper 598.
Simon, A., Collison, A.J.C., 2002. Quantifying the mechanical and hydrologic effects of riparian vegetation on stream-bank stability. Earth Surface Processes and Landforms, 27(5), 527–546.
Simon, A., Curini, A., Darby, S.E., Langendoen, E.J., 2000. Bank and near-bank processes in an incised channel. Geomorphology, 35(3-4), 193–217.
Simon, A., Darby, S.E., 1997. Process-form interactions in unstable sand-bed river channels: A numerical modelling approach. Geomorphology, 21, 85–106.
Simon, A., Rinaldi, M., 2006. Disturbance, stream incision, and channel evolution: The roles of excess transport capacity and boundary materials in controlling channel response. Geomorphology, 79(3-4), 361–383.
Simon, A., Thomas, R.E., 2002. Processes and forms of an unstable alluvial system with resistant, cohesive streambeds. Earth Surface Processes and Landforms, 27(7), 699–718.
Simon, A., Rinaldi, M., Hadish, G., 1996. Channel evolution in the loess area of the Midwestern United States. Proceedings, Sixth Federal Interagency Sedimentation Conference, Las Vegas, III-86-93.
Simon, A., Thomas, R.E., Curini, A., and Shields Jr., F.D., 2002. Case Study: Channel stability of the Missouri River, Eastern Montana. J. Hydraulic Engineering, ASCE, 128(10), 880–890.

Simon, A., Doyle, M., Kondolf, M., Shields Jr., F.D., Rhoads, B., McPhillips, M., 2007. Critical evaluation of how the Rosgen classification and associated “Natural Channel Design” methods fail to integrate and quantify fluvial processes and channel response. Journal of the American Water Resources Association, 43(5), 1117–1131.

Simon, A., Pollen-Bankhead, N., Thomas, R.E., 2011. Development and application of a deterministic bank stability and toe erosion model for stream restoration. In: Stream Restoration in Dynamic Fluvial Systems: Scientific Approaches, Analyses, and Tools, American Geophysical Union, Geophysical Monograph Series 194. pp. 453-474.

Terzaghi, K., Peck, R.B., 1967. Soil mechanics in engineering practice, Second edition. John Wiley & Sons, Inc., New York, NY.

van der Mark, C.F., van der Sligte, R.A.M., Becker, A., Mosselman, E., Verheij, H.J., 2012. A method for systematic assessment of the morphodynamic response to removal of bank protection. River Flow 2012, International Conference on Fluvial Hydraulics, Sept. 5-7, San Jose, Costa Rica.

White, W.R., Bettess, R., Paris, E., 1982. Analytical approach to river regime. Journal of Hydraulics Division, ASCE, 108, 1179–1193.

Wilcock, P.R., Crowe, J.C., 2003. Surface-based transport model for mixed-size sediment. J. Hydraulic Engineering, ASCE, 129(2), 120–128.

Wilkin, D.C., Hebel, S.J., 1982. Erosion, redeposition, and delivery of sediment to Midwestern streams. Water Resources Research, 18(4), 1278–1282.

Williams, G.P., 1978. Hydraulic geometry of river cross sections - theory of minimum variance. Professional Paper No.1029, US Geological Survey. 47 pp.

Yang, C.T., 1976. Minimum unit stream power and fluvial hydraulics. Journal of Hydraulics Division, ASCE, 102, 769–784.

**List of Figures**

Fig.1. Illustration of a multilayer bank with a planar failure and the vertical slice method.

Fig. 2. Schematic for the segmentation of local flow areas and hydraulic radii.

Fig. 3. Model verification case with an open channel flow through a channel: (A) initial mesh at time 0; (B) final mesh at time 1 s; (C) predicted vertical velocity contour when moving mesh is not invoked.

Fig. 4. The solution domain, the 2D mesh, and initial bathymetry in March 1996 for the Goodwin Creek modeling; the outer red box represents the bank zone, 11 red lateral lines represent the bank profile for retreat modeling, and black dots are the 11 cross section survey points.

Fig. 5. Recorded flow discharge through the bend and the stage at XS-11 computed from the rating curve (Q1, Q2, and Q5 refer to the 1-, 2-, and 5-year recurrence discharges).

Fig. 6. Bank profile and its layering (stratigraphy) at XS-6.

Fig.7. Comparison of predicted and measured bank top retreat from March 1996 to February 2001.

Fig. 8. Initial (left) and final (right) meshes with the 2D model and the bed elevation (black box on the right is the initial right bank boundary).

Fig. 9. Comparison of predicted (solid lines) and measured (dash lines with symbols) bank retreat at cross sections 4 to 9 (the same color corresponds to the same time).

Fig. 10. Sensitivity of bank retreat to the groundwater elevation.

Table 1

Size range of each sediment size class and the compositions of initial bed sediment and all layers of the bank profile at XS-6

| Size range (mm) | <0.01 | 0.01-0.0625 | 0.0625-0.25 | 0.25-1.0 | 1-2 | 2-8 | 8-16 | 16-32 | 32-128 |
|---|---|---|---|---|---|---|---|---|---|
| Initial bed | 0.0017 | 0.0048 | 0.013 | 0.276 | 0.061 | 0.1756 | 0.1654 | 0.21 | 0.0925 |
| Layer 1 | 0.1177 | 0.7546 | 0.0995 | 0.0141 | 0.014 | 0.0001 | 0 | 0 | 0 |
| Layer 2 | 0.1177 | 0.7564 | 0.0995 | 0.0141 | 0.014 | 0.001 | 0 | 0 | 0 |
| Layer 3 | 0.1164 | 0.3554 | 0.257 | 0.13 | 0.1207 | 0.0205 | 0 | 0 | 0 |
| Layer 4 | 0 | 0 | 0.2 | 0.16 | 0.14 | 0.3 | 0.15 | 0.05 | 0 |

Table 2

Bank stratigraphy and geotechnical properties at bank profile XS-6

| Layer | Depth below surface | Porosity | Saturated unit weight ($kNm^{-3}$) | Friction angle (°) | Angle $\phi^b$ (°) | Cohesion (kPa) |
|---|---|---|---|---|---|---|
| 1 | 0–0.5 | 0.489 | 16.9 | 33.1 | 17.0 | 1.41 |
| 2 | 0.5-1.7 | 0.489 | 19.3 | 28.1 | 10.2 | 2.70 |
| 3 | 1.7-3.2 | 0.380 | 19.9 | 27.0 | 17.0 | 6.30 |
| 4 | >3.2 | 0.320 | 21.0 | 35.0 | 17.0 | 1.00 |

Table 3
Predicted and observed top channel width in March 2001 for cross sections 4-9 along the Goodwin Creek site

| Cross section | Predicted top width (m) in March 2001 | Observed top width(m) in March 2001 | Absolute error (m) | Relative error (%) | Predicted top width (m) in March 2001 with 1D model (Langendoen and Simon, 2008) |
|---|---|---|---|---|---|
| 4 | 30.70 | 31.65 | -0.95 | -3.0 | 31.13 |
| 5 | 30.58 | 30.50 | 0.08 | 0.26 | 29.71 |
| 6 | 31.55 | 31.30 | 0.25 | 0.80 | 31.39 |
| 7 | 30.78 | 30.73 | 0.05 | 0.16 | 30.72 |
| 8 | 34.41 | 32.71 | 1.70 | 5.2 | 30.99 |
| 9 | 27.84 | 26.89 | 0.95 | 3.5 | 26.86 |
| Average | 30.98 | 30.63 | 0.66 | 2.2 | 30.26 |

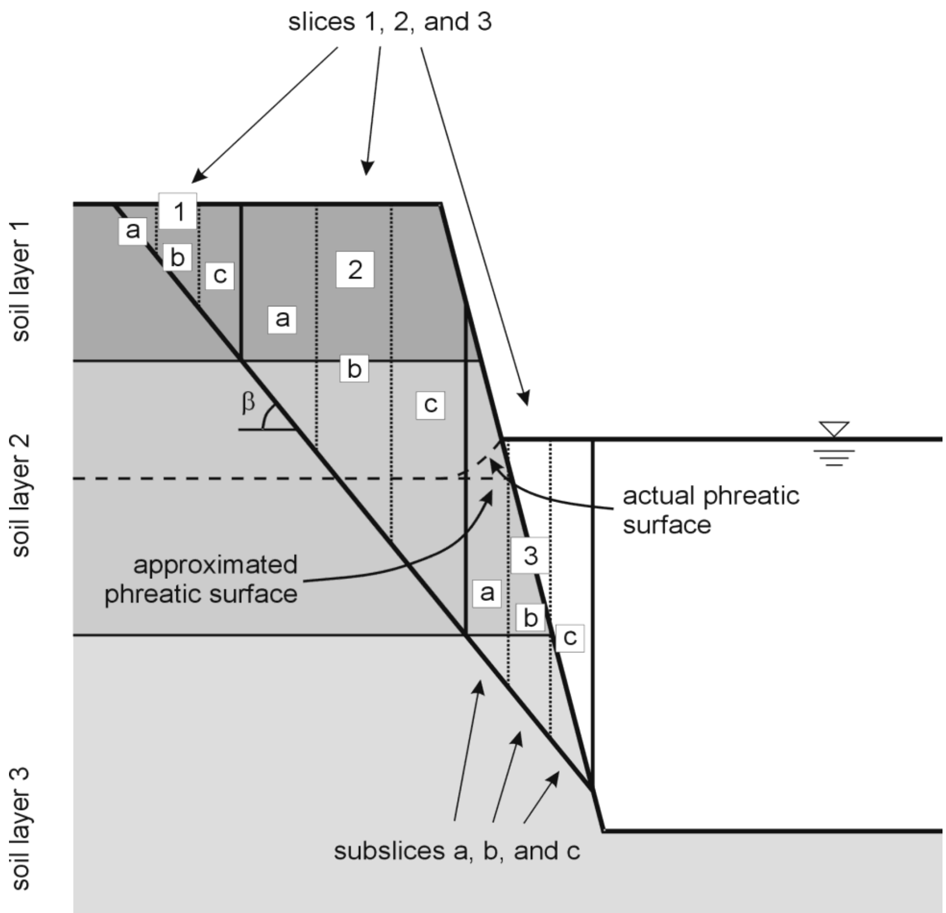
slices 1, 2, and 3
soil layer 1
soil layer 2
soil layer 3
1
2
3
a
b
c
a
b
c
a
b
c
β
actual phreatic
surface
approximated
phreatic surface
subslices a, b, and c

Fig. 1

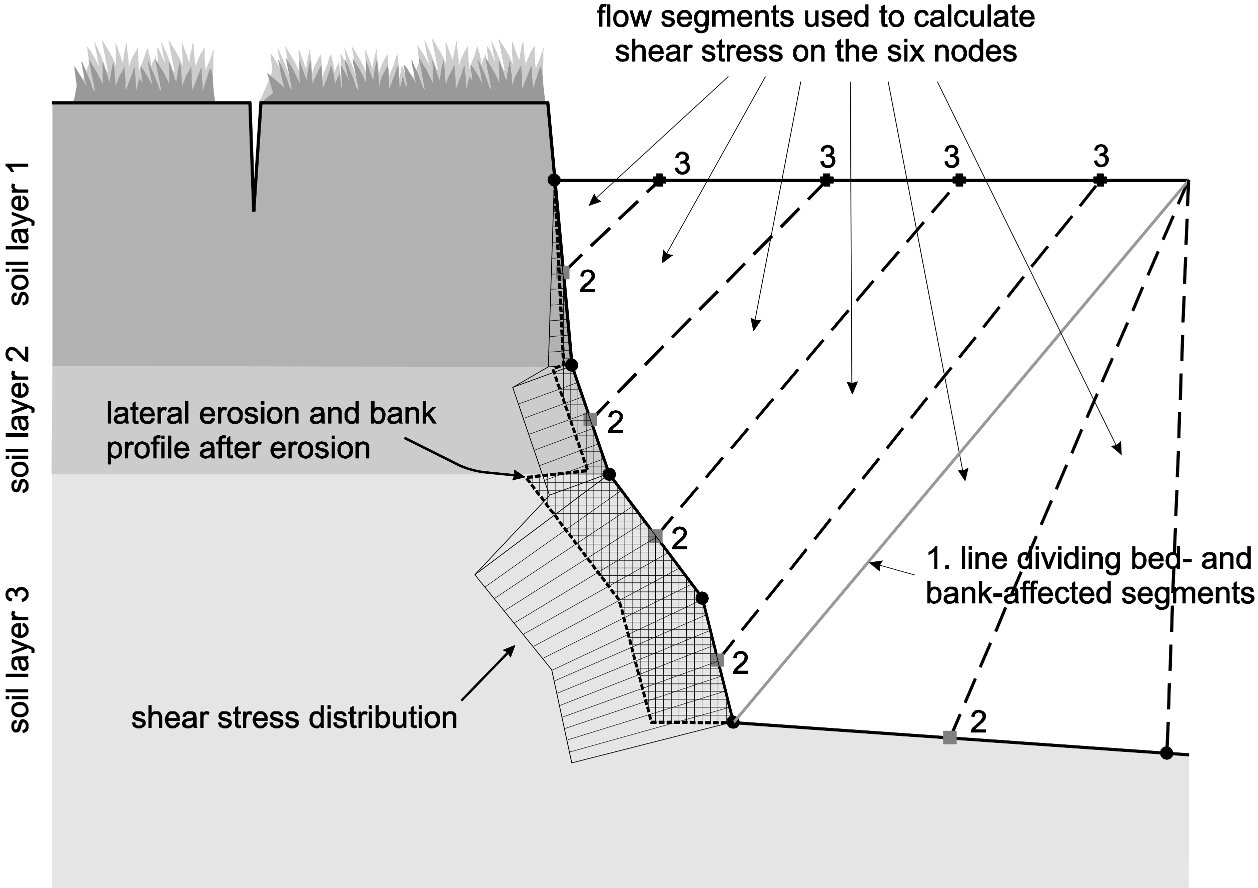
flow segments used to calculate
shear stress on the six nodes
soil layer 1
soil layer 2
soil layer 3
3
3
3
3
2
2
2
2
2
lateral erosion and bank
profile after erosion
1. line dividing bed- and
bank-affected segments
shear stress distribution

Fig. 2

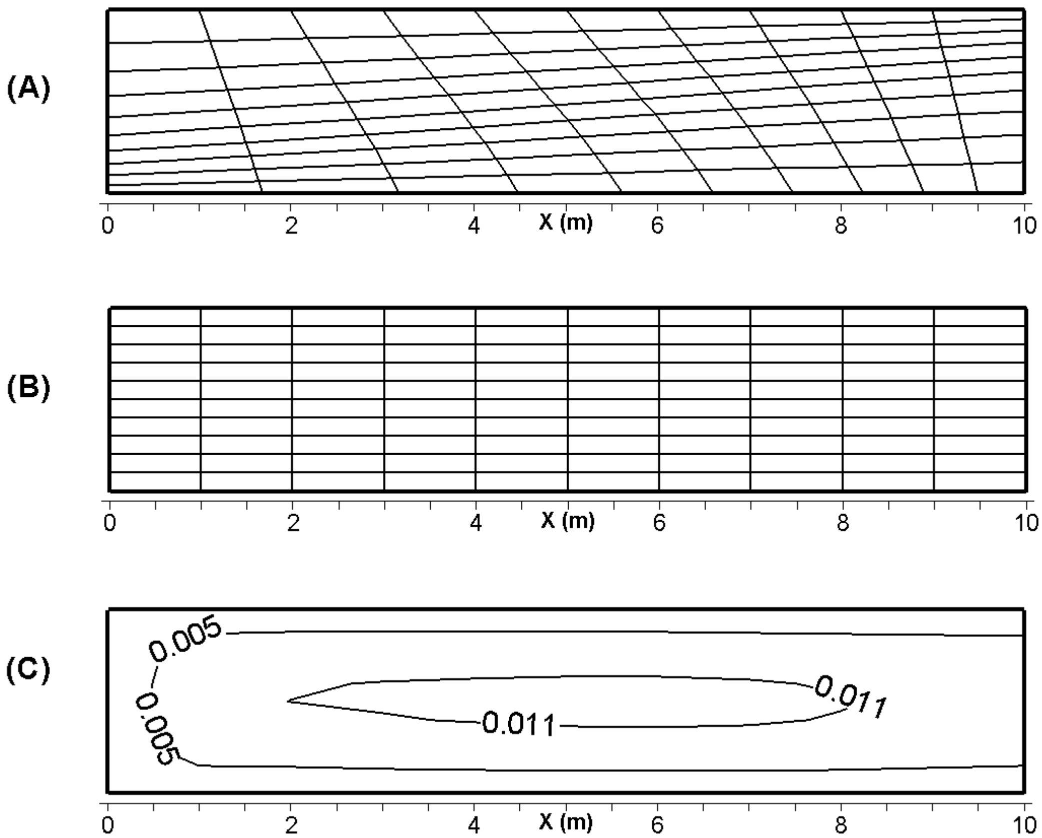


Fig. 3

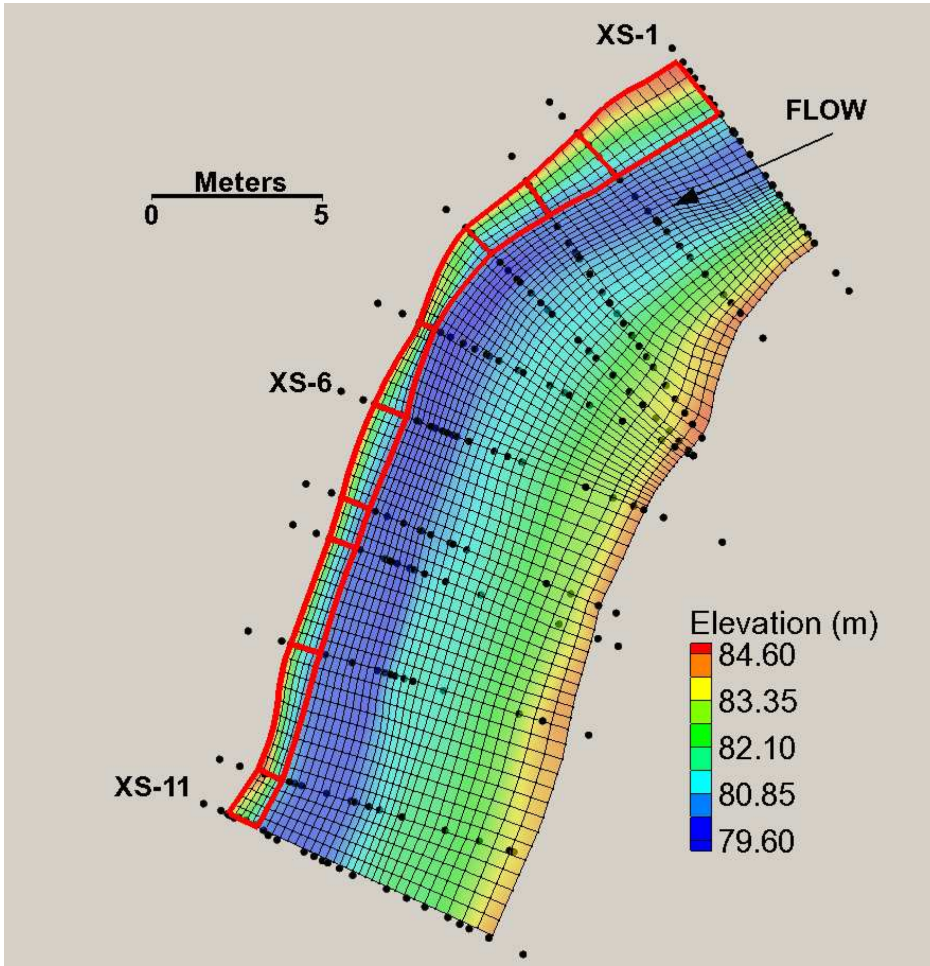
XS-1
FLOW
Meters
0
5
XS-6
XS-11
Elevation (m)
84.60
83.35
82.10
80.85
79.60

Fig. 4

(A) Discharge at Upstream (B) Stage at XS 11

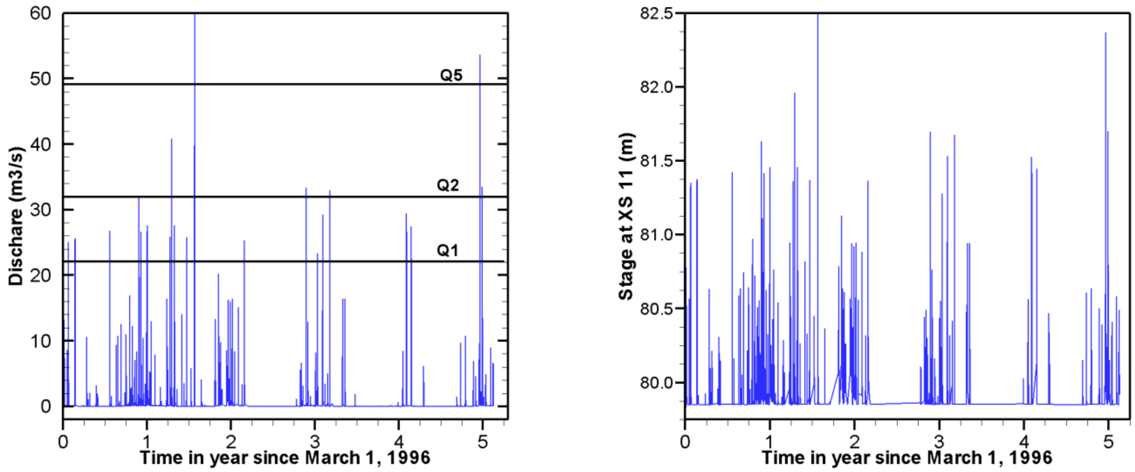


Fig. 5

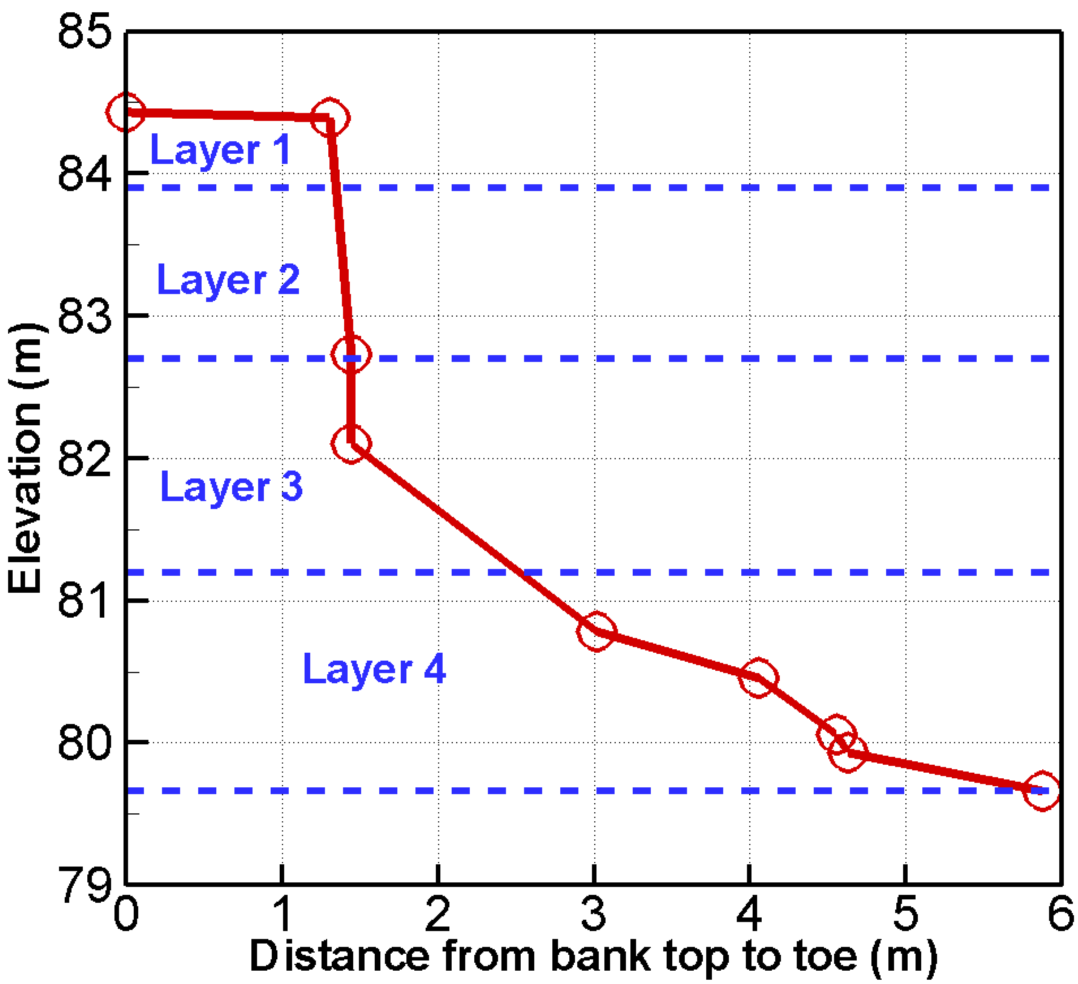
85
84
83
82
81
80
79
Elevation (m)
Layer 1
Layer 2
Layer 3
Layer 4
0
1
2
3
4
5
6
Distance from bank top to toe (m)

Fig. 6

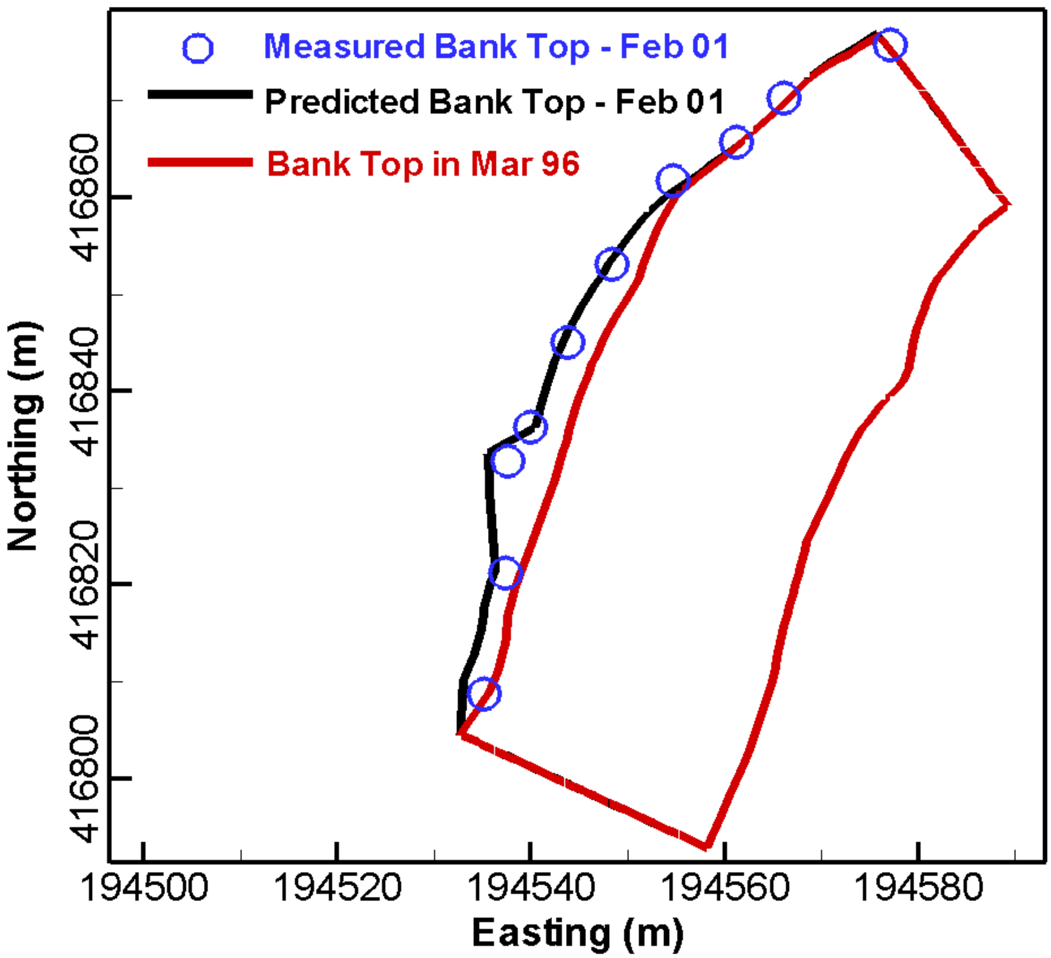
Measured Bank Top - Feb 01
Predicted Bank Top - Feb 01
Bank Top in Mar 96
Northing (m)
416800
416820
416840
416860
Easting (m)
194500
194520
194540
194560
194580

Fig. 7

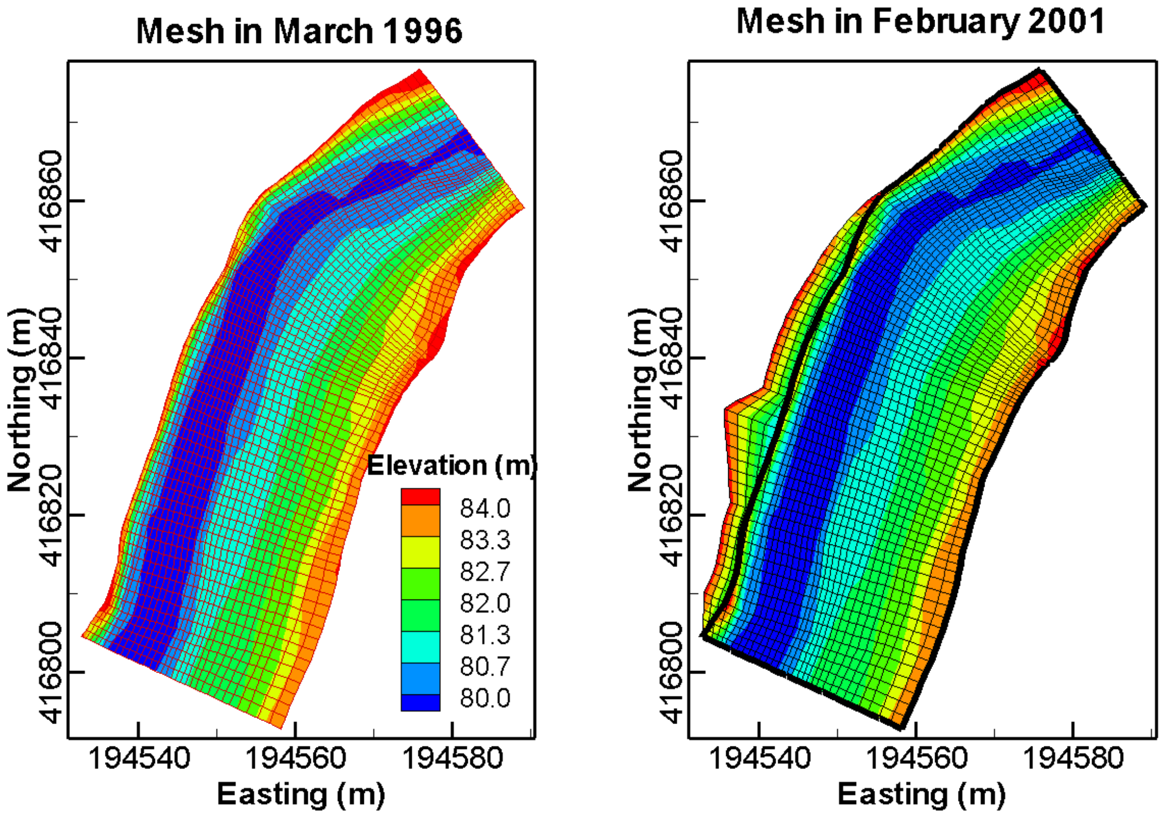
Mesh in March 1996
Mesh in February 2001
Northing (m)
416800
416820
416840
416860
Easting (m)
194540
194560
194580
Elevation (m)
84.0
83.3
82.7
82.0
81.3
80.7
80.0

Fig. 8

1024

(A) XS 4

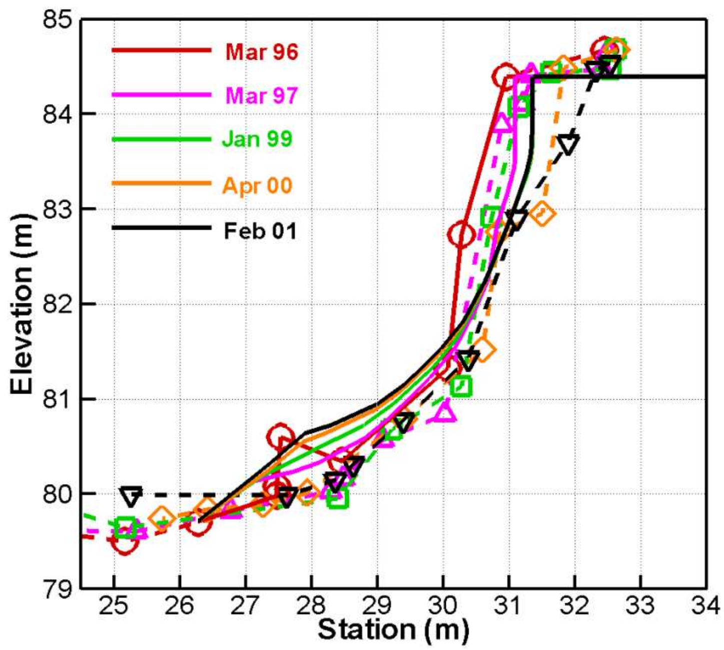


(B) XS 5

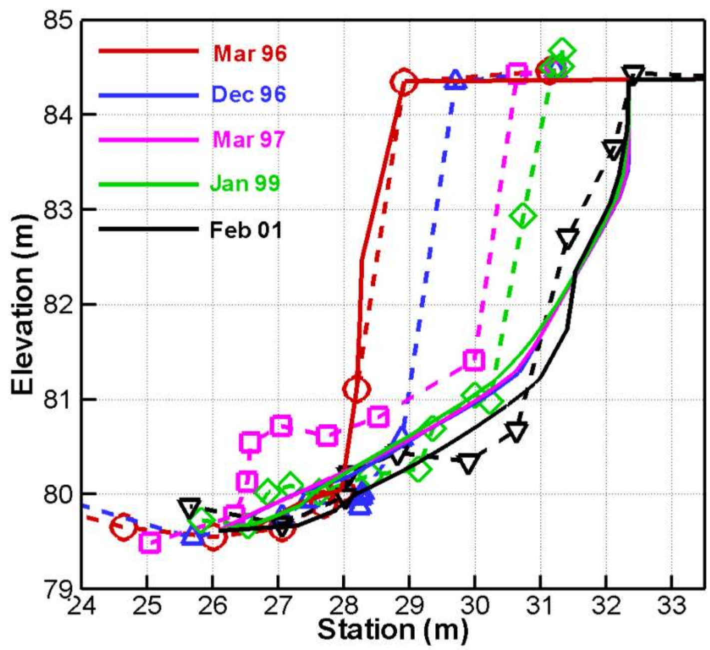

(C) XS 6

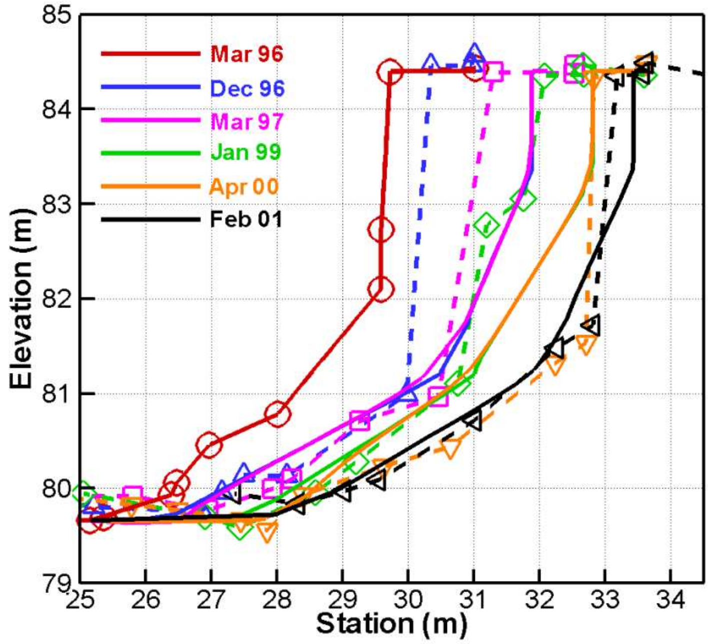
Mar 96
Dec 96
Mar 97
Jan 99
Apr 00
Feb 01
Elevation (m)
Station (m)
85
84
83
82
81
80
79
25
26
27
28
29
30
31
32
33
34

(D) XS 7

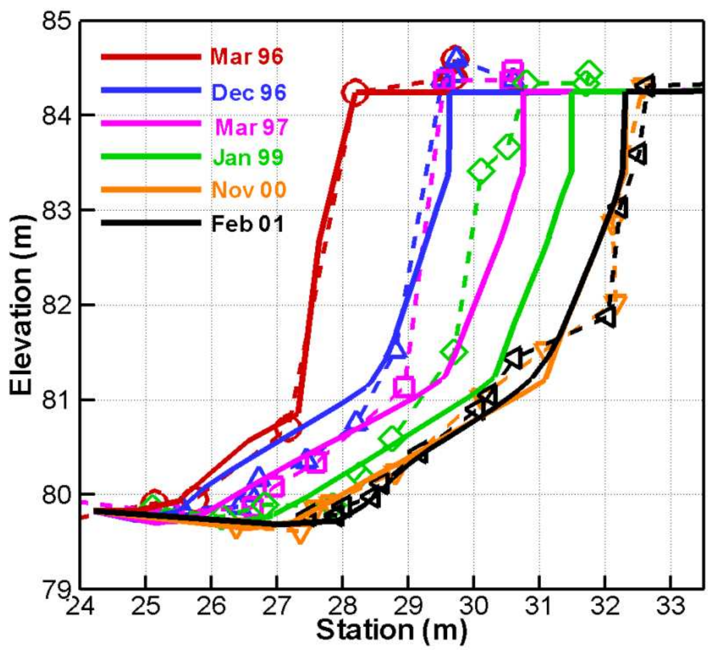
Mar 96
Dec 96
Mar 97
Jan 99
Nov 00
Feb 01
Elevation (m)
Station (m)
85
84
83
82
81
80
79
24
25
26
27
28
29
30
31
32
33

(E) XS 8

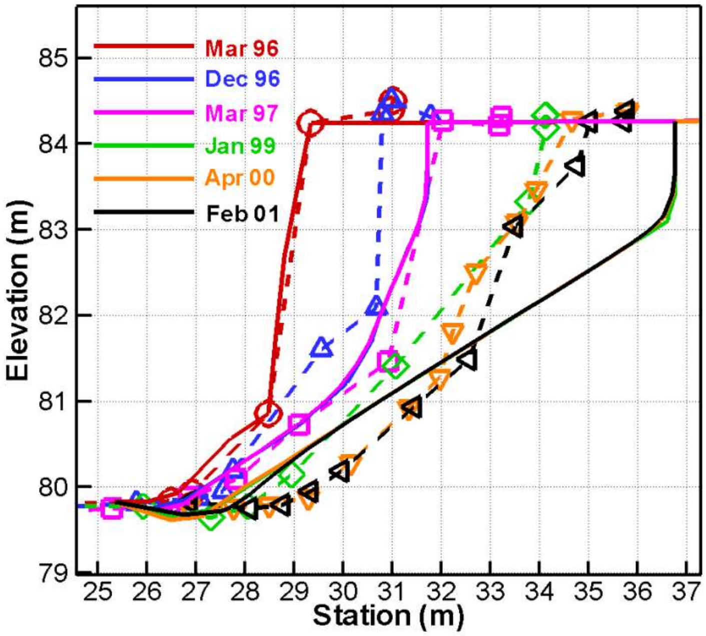


(F) XS 9

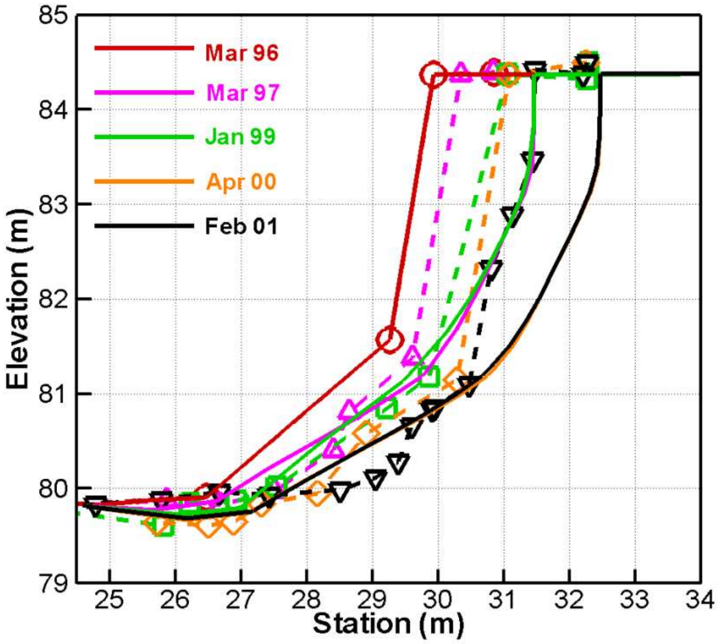


Fig. 9

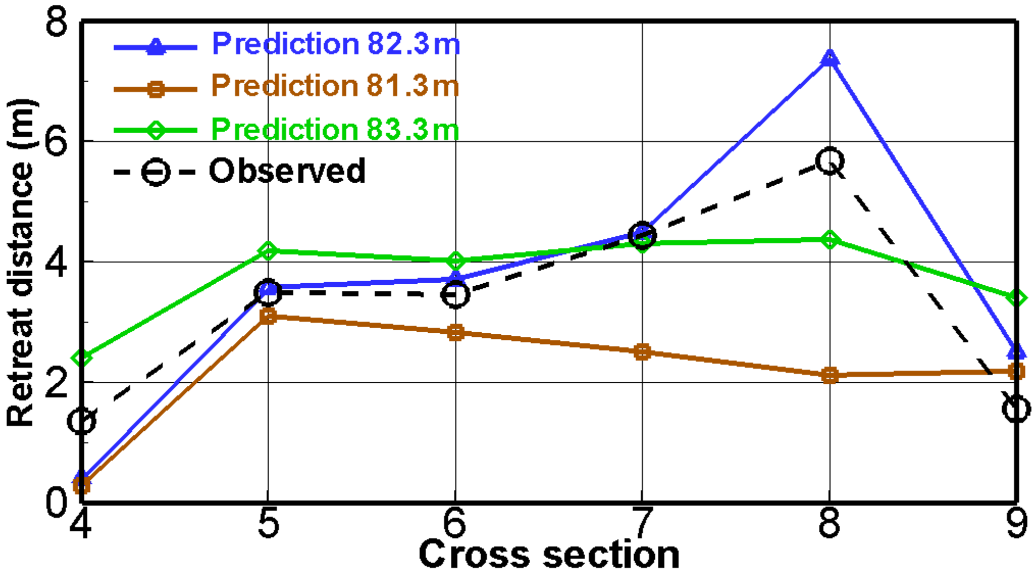
Prediction 82.3m
Prediction 81.3m
Prediction 83.3m
Observed
Retreat distance (m)
0
2
4
6
8
4
5
6
7
8
9
Cross section

Fig. 10